JOURNAL OF GEOPHYSICAL RESEARCH, VOL. 86, NO. A13, PAGES 11,401–11,418, DECEMBER 1, 1981

Solar Wind Flow About the Terrestrial Planets
1. Modeling Bow Shock Position and Shape

JAMES A. SLAVIN AND ROBERT E. HOLZER

Institute of Geophysics and Planetary Physics, University of California at Los Angeles, Los Angeles, California 90024

General technique for modeling the position and shape of planetary bow waves are reviewed. A three-parameter method was selected to model the near portion (i.e., $x' > -1 R_{ob}$) of the Venus, earth, and Mars bow shocks and the results compared with existing models using 1 to 6 free variables. By limiting consideration to the forward part of the bow wave, only the region of the shock surface that is most sensitive to obstacle shape and size was examined. In contrast, most other studies include portions of the more distant downstream shock, thus tending to reduce the planetary magnetosphere in question to a point source and constrain the resultant model surfaces to be paraboloid or hyperboloid in shape to avoid downstream closure. It was found by this investigation that the relative effective shapes of the near Martian, Cytherean, and terrestrial bow shocks are ellipsoidal, paraboloidal, and hyperboloidal, respectively, in response to the increasing bluntness of the obstacles that Mars, Venus, and earth present to the solar wind. The position of the terrestrial shock over the years 1965 to 1972 showed only a weak dependence on the phase of the solar cycle after the effects of solar wind dynamic pressure on magnetopause location were taken into account. However, the bow wave of Venus was considerably more distant around solar maximum in 1979 than at minimum in 1975–6 suggesting a solar cycle variation in its interaction with the solar wind. Finally, no significant deviations from axial symmetry were found when the near bow waves of the earth and Venus were mapped into the aberrated terminator plane. This finding is in agreement with the predictions of gas dynamic theory which neglects the effects of the IMF on the grounds of their smallness. Farther downstream where the bow wave position is being limited by the MHD fast mode Mach cone, an elliptical cross section is expected and noted in the results of other investigations.

INTRODUCTION

Among the major early discoveries of the space program was the presence of a bow shock upstream of the earth (e.g., *Spreiter and Alksne* [1970], *Dryer* [1970], and references therein). Given the large collisional mean free path of solar wind particles (i.e., $\lambda \sim 1$ AU) it might have been expected at the time that the magnetosphere would represent a small (i.e., $\sim 10^{-3}$ λ) scattering center as opposed to an obstacle deflecting fluid through the formation of a standing bow wave. Thus planetary bow shocks comprise some of our earliest, and perhaps most striking, observational evidence for the existence of the microscale plasma processes that allow the solar wind to exhibit bulk fluid properties on spatial scales much smaller than the physical dimensions of the planets. Further, the thickness of the transition layer within which a portion of the plasma flow energy is converted to internal energy, turbulence, waves, and suprathermal particles has been found to be small in comparison with the shock stand-off distance. Hence, the bow wave may, for some purposes, be considered a mathematical discontinuity as has been done in obtaining both gasdynamic [*Spreiter and Jones*, 1963; *Dryer and Faye-Petersen*, 1966; *Spreiter et al.*, 1966; *Dryer and Heckman, 1967; Spreiter and Stahara*, 1980*a*, *b*] and MHD [*Spreiter and Rizzi*, 1974] solutions to the continuum description.

These remarks find relevance in Figure 1 which brings together samples of the shock observations that have been made at each of the terrestrial planets: Mercury [*Ness et al.*, 1975], Venus [*Slavin et al.*, 1980], earth [*Russell and Greenstadt*, 1979], and Mars [*Smith*, 1969]. Magnetometer observations are preferentially displayed here because of their ability to make high time resolution (e.g., 1–10 Hz) measurements relative to those of the plasma instruments. However, with some exceptions that will be discussed later, there is generally good agreement among the particles and fields experiments as to the location of the shock over length scales greater than the transition layer thickness, $\sim c/\omega_{pi}$ [e.g., *Vaisberg*, 1976; *Ogilvie et al.*, 1977; *Russell and Greenstadt*, 1979; *Slavin et al.*, 1980]. The magnetic field observations in Figure 1 show a series of quasi-perpendicular shock crossings by, from top to bottom, Mariner 10, Pioneer Venus, Isee 1, and Mariner 4. In each case the upstream precursors are quite small in amplitude, the transition layer thickness on the order of the ion inertial length, and the jump in the field magnitude strong (i.e., approaching $(\gamma + 1)/(\gamma - 1)$ for the transverse component). Under these favorable conditions, bow shock crossings may be unambiguously identified in the experimental data records with precision limited only by the instrument sampling rate and the relative velocity of the shock. However, it must be noted that the determination of bow wave location is complicated on occasion by "quasi-parallel" conditions when the angle between the shock surface normal and the upstream interplanetary magnetic field becomes small. In these instances there is a broadening of the region over which the plasma is "shocked" and an increase in turbulence both upstream and downstream [e.g., *Greenstadt*, 1970] making a judgement as to the shock location less certain and sometimes difficult in the absence of plasma as well as magnetic field data. However, the relative number of passes during which a distinct crossing fails to be recorded is not large [e.g., *Fairfield*, 1971; *Olson and Holzer*, 1975] and the study of minor changes in shock position as a function of its structure [*Formisano et al.*, 1973; *Auer*, 1974] is outside the intended domain of this work. Accordingly, the results of this study may not be strictly applicable to the highly quasi-parallel portions of planetary bow waves. Observations have also shown that shock motion may occur at speeds of $10-10^2$ km/s [*Holzer et al.*, 1966; *Greenstadt et al.*, 1972] in response to changing upstream parameters and interactions with solar wind discontinuities to produce multiple encounters between spacecraft and the shock even when the probe velocity is as great as ~ 11 km/s such as was the case for Mariner 10 at the time of the observations in Figure 1. The treatment of multiple encounters in boundary mapping problems varies from study to study and is considered in the next section. Mean values of the various interplanetary parameters change with distance from the sun as can be seen, for example, in

Paper number 1A1147.
0148-0227/81/001A-1147 $01.00

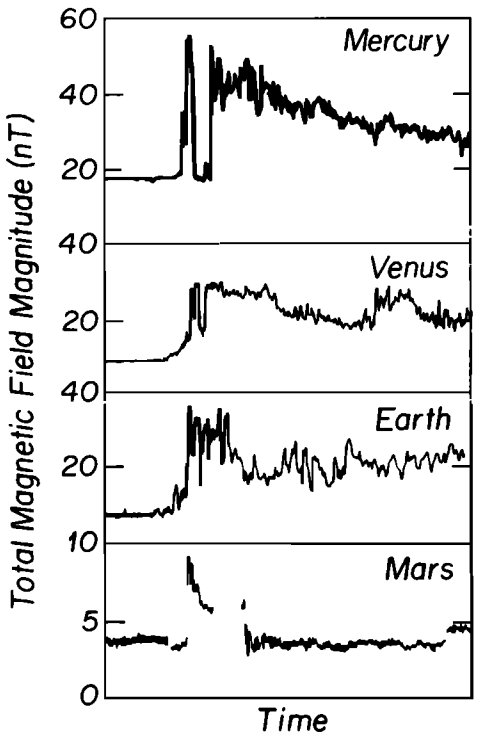

Fig. 1. Quasi-perpendicular bow shocks at Mercury, Venus, Earth, and Mars are displayed as adapted from *Ness et al.* [1975], *Slavin et al.* [1980], *Russell and Greenstadt* [1970], and *Smith* [1969]. In time the top 3 panels span several minutes each, while the Mars encounter covers about 12 hours. Multiple encounters due to shock motion are evident in the Mercury and Venus profiles. The time spent in the magnetosheath at Mars appears small owing to the compressed time scale and the grazing nature of the high-altitude Mariner 4 fly-by as well as any variations associated with bow wave motion at the time of the meaurements (Note: *Greenstadt* [1970] has determined that the final (i.e., exit) shock crossing at Mars may have fulfilled the requirements for being quasi-parallel.)

the decrease in the total upstream magnetic field magnitude in Figure 1 from almost 20 nT at Mercury (i.e., 0.46 AU) to below 5 nT at Mars (i.e., 1.52 AU). However, the alterations in the relevant quantities such as the IMF spiral angle, sonic and Alfvénic Mach numbers, or others appearing in Tables 1 and 2 are not large in comparison with the statistical deviations about their mean levels and have not been found to result in any substantial differences in shock structure among these planets [*Greenstadt*, 1970; *Fairfield and Behannon*, 1976; *Slavin et al.*, 1980] as is evident from the very similar quasi-perpendicular magnetic field profiles assembled in Figure 1.

What has been found to vary from planet to planet is the nature of their respective interactions with the solar wind and hence the various aspects of flow about these bodies. For this reason it would be highly desirable to explore the region between the bow wave and the dense lower atmosphere of each planet with particles and fields experiments. However, such programs have been restricted largely to the earth. Further, the examination of flow through any volume, such as the magnetosheath, is limited to statistical studies if the boundary location and boundary conditions are not known at the time of the individual observations as is the case with single spacecraft measurements [e.g., *Hundhausen et al.*, 1969; *Howe and Binsack*, 1972]. Owing to the natural variability of the solar wind and the planetary response both the bow shocks and the magneto/ionopauses of planets are in nearly continuous motion [e.g., *Holzer et al.*, 1966; *Slavin et al.*, 1980]. This point is illustrated not only by the multiple boundary crossings in Figure 1, but also Figure 2, which plots average daily location of the Venus bow shock mapped into the solar wind aberrated terminator plane as observed by Pioneer Venus during its first 225 days in orbit. As is the case at the earth, large fluctuations are present. They have been studied by *Slavin et al.* [1979*a*,*b*; 1980] and attributed to changes in not only ionopause height and solar wind Mach number, but also the solar wind interaction through the effects of varying solar corpuscular and electromagnetic radiation on the ionosphere and neutral atmosphere. At Mercury and Mars still less data are available with none of it having been taken at low altitudes on the dayside (see reviews by *Ness* [1979], *Russell* [1979], and *Siscoe and Slavin* [1979]). Hence, at this time the study of solar wind flow about these planets as a group is still reduced the temporal variability of these physical systems, the overall paucity of observations, and the limitations of single spacecraft measurements to an examination of bow wave position, shape, and variability.

In this paper we report on the findings of the first of the two part study of this subject. As will be described below, Part 1 models the shape and location of the bow waves of Venus, earth, and Mars by a single standard technique for the purpose of comparing their relative shapes and positions. This is in contrast to the many other studies [e.g., *Bogdanov and Vaisberg*, 1975; *Vaisberg*, 1976; *Russell*, 1977; *Verigin et al.*, 1978] that have considered different aspects of this problem but with fewer observations and in less comprehensive and methodical manners than employed here. Figure 3 shows the timing of the various space missions that will be used relative to the sunspot cycle. The reason for such a display is that the interplanetary medium appears to exhibit variations with solar cycle phase [e.g., *Diodato et al.*, 1974; *King*, 1979] which are known to affect the nature of solar wind interaction with the earth (e.g., *Holzer and Slavin* [1981] and references therein). Similar modulations are also expected at the other planets but so far have been reported on the basis of in situ observations only at Venus [*Wolff et al.*, 1979; *Slavin et al.*, 1979*b*]. Since the various missions to Mercury, Venus, and Mars have occurred at different times with respect to the solar cycle, observations of the terrestrial bow wave

TABLE 1. Interplanetary Conditions

Planet	R, AU	V_{sw}, Km/S	n_p, cm^{-3}	B, nT	T_p, 10^4°K	T_e, 10^4°K
Mercury	0.31	430	73	46	17	22
	0.47	430	32	21	13	19
Venus	0.72	430	14	10	10	17
Earth	1.00	430	7	6	8	15
Mars	1.52	430	3.0	3.3	6.1	13
(Scaling)	•••	R°	R^{-2}	$R^{-1}(2R^{-2}+2)^{1/2}$	$R^{-2/3}$	$R^{-1/3}$

A set of 'typical' long term mean parameters at 1 AU have been scaled to the orbits of the other terrestrial planets by using the approximate radial dependencies displayed in the last row. The least certain scalings are those for temperature where the values of *Gazis et al.* [1981] for T_p and *Sittler and Scudder* [1980] for T_e have been adopted.

TABLE 2. Bow Wave Parameters

Planet	R, AU	P_{sw}, 10^{-8} dynes/cm^2	M_s	M_A	β	Q	c/ω_{pi}, km	Spiral Angle, deg
Mercury	0.31	26	5.5	3.9	0.5	15	27	17
	0.47	11	6.1	5.7	0.9	32	40	25
Venus	0.72	5.0	6.6	7.9	1.4	62	61	36
Earth	1.00	2.5	7.2	9.4	1.7	88	86	45
Mars	1.52	1.1	7.9	11.1	2.0	120	130	57

Using the basic parameters from the first table a series of plasma quantities relevant to planetary bow shocks have been computed; $P_{sw} = 1.16 n_p m_p V_{sw}^2$, $M_s = V_{sw}/(2k_B(1.14T_p + 1.08T_e)/1.16m_p)^{1/2}$, $M_A = V_{sw}(1.16 n_p m_p 4\pi)^{1/2}/B$, $\beta = 8\pi n_p k_B(1.14T_p + 1.08T_e)/B^2$, $Q = M_A = \frac{1}{2}P_{sw}8\pi/B^2$, $c/\omega_{pi} = 228/n^{1/2}$, and IMF spiral angle = $\tan^{-1}(R)$. In all cases, the solar wind plasma has been assumed to contain 4% He^{++} with $T_{He} = 3.5T_p$.

from a series of five satellites spanning most of cycle 20 were selected as a control group against which the more limited Mars and Venus measurements will be compared. Part 2, which is in preparation, examines the ability of existing gasdynamic and MHD models to describe the mean flow conditions as implied by shock location and makes use of these models in a comparative study of the solar wind interaction with the terrestrial planets. Mercury has been for the most part excluded from this modeling study due not only to the limited amount of data collected during the Mariner 10 fly-bys but also because those encounters may have taken place during abnormal interplanetary and magnetospheric conditions (*Slavin and Holzer* [1979] and references therein). While Mariner 10 provided a wealth of information on the basic nature of the solar wind interaction with the Hermaean magnetosphere, its observations are insufficient to give us a view of shock shape and stand-off distance under the typical 0.3–0.5 AU interplanetary parameters shown in Table 2. Examination of Jupiter and Saturn has been deferred until the large body of Voyager observations at Jupiter and Saturn are more fully reduced and disseminated.

MODELING THE BOW SHOCK

The ideal experiment to determine the shape and location of the bow shock for a given set of interplanetary and obstacle conditions would involve a large number of probes simultaneously crossing the boundary at near normal incidence angles with high relative speeds to obtain a "snapshot" of the shock surface. In the absence of such an experiment, the next choice would be to follow the trajectories of a large number of satellites through a three-dimensional grid classifying each unit volume as being located in the magnetosphere, magnetosheath, or solar wind. In principal, the locations of the magnetopause and bow wave could then be recovered both in the mean and under specific conditions through appropriate selection, averaging, and weighting of the data. The main advantage of such an approach is that all of the information gathered, as opposed to just the boundary crossings, may be used in formulating probability distributions for boundary location. However, its usefulness is limited by the need for a statistically significant number of observations per unit volume. The resultant grid at this time is still too large to be of use in studying the shock location. At some future date this will, hopefully, no longer be the case.

For the reasons given above, the approach used since the beginning of such studies is to identify shock crossings in the particles and field observations and utilize curve fitting techniques to model location and shape. Its principle disadvantage is that care must be exercised in data selection to avoid producing a spatially biased representation. In general, shock observations taken along satellite trajectories that make a small angle with the boundary surface and/or do not begin well below (above) and end well above (below) the altitudes at which the shock resides must be omitted. There is

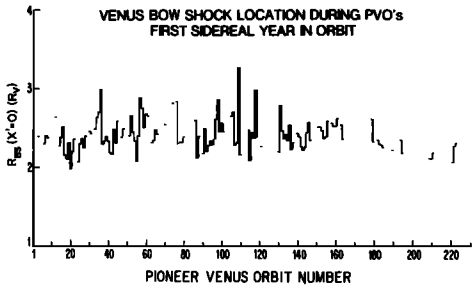

Fig. 2. With its 24-hour orbit the Pioneer Venus orbiter crosses the bow shock twice daily except occasionally when apoapsis is near local midnight and the spacecraft doesn't get far enough away from the x' axis to penetrate into the solar wind. Displayed above are the bow shock crossings from *Slavin et al.* [1980]. They have been mapped into the aberrated terminator plane by using the model surface from that study with the daily average distance from the center of the planet to the shock plotted against orbit number (Note: Orbit 1 = December 5, 1978).

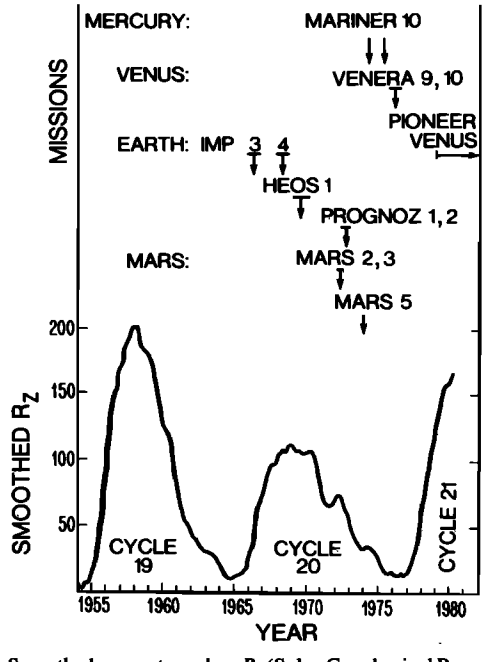

Fig. 3. Smoothed sunspot number, R_z (Solar-Geophysical Reports, 1980), and the active periods of the various planetary missions used in this work to model bow waves are plotted against time. As shown, Pioneer Venus orbiter may offer our first opportunity to study the solar wind interaction with a planet other than earth over a complete solar cycle.

TABLE 3. Summary of Principal Earth Bow Shock Models (Cartesian Form)

Study	S/C	#Passes	Period	Domain	k_1	k_2	k_3	k_4	k_5	k_6
Fairfield [1971]										
'Meridian 4°'	Imp 1									
	Imp 3									
	Imp 4									
	Exp 33									
	Exp 35	389	1963–8	$x \quad -45R_e$	1	0.0296	−0.0381	−1.280	45.644	−652.10
'Meridian NO 4°'	Same	Same	Same	Same	1	0.2012	−0.1023	−4.76	44.466	−629.03
'X ROT. NO 4°'	Same	Same	Same	Same	1	0.2164	−0.0986	−4.26	44.916	−623.77
Formisano [1979] (With $\bar{z} = 0$)										
'P_{sw} Unnormalized'	Imp 1									
	Imp 3									
	Imp 4									
	Exp 33									
	Heos 1									
	Heos 2	700	1963–73	Same	1	0.12	0.06	−4.92	43.9	−634
'P_{sw} Normalized'	Same	~450	Same	Same	1	0.18	0.45	−4.16	46.6	−618

Information on the respective bow shock data sets of Fairfield and Formisano is presented and the resultant coefficients for their second order surfaces listed. While the data set of Formisano is that of Fairfield with Heos 1 and 2 crossings added, no exact number of passes is available for the Formisano study because each shock encounter was considered separately. In addition, the Formisano models were three dimensional so that for the sake of the comparisons conducted in this investigation only the traces of his models in the ecliptic plane are considered (i.e., $z = 0$).

also the question of multiple crossings with the shock on a single orbit that can take place at the earth, for example, over distances of many planetary radii. It has been the policy of this study to fit the average shock location per inbound or outbound orbit leg as is generally done [e.g., *Holzer et al.*, 1966; *Fairfield*, 1971]. The reason for this decision is that the individual multiple encounters are not usually statistically independent of each other with respect to obstacle and solar wind conditions. Multiple encounters with the shock may take place over intervals of many hours, but are often separated by only minutes, or less. By comparison, the interplanetary parameters are most commonly available as 1- to 3-hour averages [*King*, 1977] and are statistically independent only over periods of tens of hours, or more, depending upon the physical variable considered [e.g., see *Gosling and Bame*, 1972; *King*, 1979]. Further, the rate of occurrence of multiple crossings will vary with the individual spacecraft trajectory and tend to bias the data set by more heavily weighting the less desirable observations made along orbits with smaller incidence angles to the boundary surface due to the large number of encounters generated by small amplitude shock motions. An excellent example of such a problem is contained in the study of shock position by *Formisano* [1979] in which the Heos 2 contributes ~80% of the total number crossings even though it completed less than half as many orbits as the total for the other 6 satellites utilized in that work combined. To avoid this domination of the data set by the Heos 2 multiple crossings and still use these important high latitude observations, weighting factors were introduced as described in that paper.

Before continuing further, it is necessary to select the coordinate space in which to model the shock surface. The most common practice is to use planet centered solar ecliptic coordinates (x, y, z) in which x points toward the sun and z is normal to the plane of the ecliptic with z positive in the same sense as the angular momentum vector of the sun [e.g., *Fairfield*, 1971; *Formisano*, 1979]. Alternatively, at the earth phenomena which are highly dependent upon the tilt of the geomagnetic field in planes perpendicular to the x axis use the geocentric solar magnetospheric system which "rocks" the $y-z$ axis with the dipole. However, except for possibly at high latitudes, which will not be considered in this study, the influences on the long term mean shock location of such phenomena are expected, consistent with previous analyses [*Gosling et al.*, 1967], to be small. Of far greater importance is "aberration" due to the orbital motion of each planet which makes the apparent direction of the average solar wind velocity of the planetary rest frame deviate from the anti-sunward direction. Past studies, such as *Fairfield* [1971] and *Formisano* [1979], have usually taken the approach of fitting the shock crossings in unaberrated solar ecliptic coordinates. The orientation of the best fit is then interpreted in terms of the average effects of aberration and other phenomena which might produce a lack of symmetry about the x axis. However, as the solar wind speed is variable we can reduce "noise" associated with aberration by aberrating each individual shock crossing at a position (x, y, z) relative to a planet with a mean orbital speed of V_p during a period of solar wind speed V_{sw} (V_{sw} = 430 km/s assumed in the absence of upstream solar wind observations) into a new space where

$$\begin{aligned} r &= \sqrt{x^2 + y^2} \\ \alpha &= \tan^{-1}(V_p/V_{sw}) + \cos^{-1}(x/r) \qquad y > 0 \\ \alpha &= \tan^{-1}(V_p/V_{sw}) - \cos^{-1}(x/r) \qquad y < 0 \\ x' &= r \cos \alpha \\ y' &= r \sin \alpha \\ z' &= z \end{aligned} \tag{1}$$

Thus in the examination to follow all shock encounters are modeled in the aberrated solar ecliptic system (x', y', z'). It would also be desirable to use the actual observed direction of the solar wind velocity. The velocity vector often does deviate from the anti-sunward direction by a few degrees, but these vector measurements are often not readily available and the effect is not as large as aberration with the mean contribution to shock orientation near zero [e.g., *Wolfe*, 1972].

Also of great importance in modeling shock location is the nature of the symmetry assumptions involved. The reason for introducing such assumptions is always, ultimately, the desire to increase the point density by legitimate means in the light of the sparse coverage of the boundary in three dimensions even at the earth. Of the past

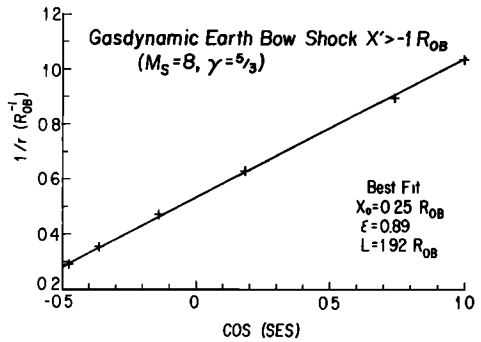

Fig. 4. A three parameter best fit to six points taken off the gasdynamic model of the earth bow shock by *Spreiter et al.* [1966] is shown in the $1/r - \cos\theta$ plane with distance in units of obstacle radii.

treatments, that by *Formisano* [1979] which fits the shock in three dimensions sets the least constraining requirement in that only symmetry with respect to the ecliptic plane (i.e., $z = |z|$) is assumed. *Fairfield* [1971] incorporated quasi-axial symmetry into the model by rotating the crossing locations about the x axis into the dawn (dusk) half of the $x-y$ plane when the y coordinate of the datum was negative (positive). In another model he assumed spherical symmetry for the shock surface on the dayside. These procedures were adopted by Fairfield so that any east-west asymmetry in flow about the earth might be detected. The existence of significant asymmetries associated with the spiral configuration of the IMF within the magnetosheath region have been both predicted [*Walters*, 1964] and disputed [*Shen*, 1972] on theoretical grounds as will be discussed further in a later section. Observationally, only small asymmetries beyond aberration were found in the studies by *Gosling et al.* [1967] and *Fairfield* [1971], whereas the work by Formisano produced mixed results that will be discussed later. Hence, on the basis of the Gosling et al. and Fairfield results we have assumed axial symmetry about the aberrated x axis (i.e., the x' axis) and modeled the shock in the $x' - (y'^2 + z'^2)^{1/2}$ plane. A search for biases due to violations of this symmetry was conducted without finding any significant asymmetries as will be reported in the section devoted to the subject. The advantage of our symmetry assumption is that it enhances the density of data points and thereby minimizes the problem of nonuniform coverage that can bias fitting in both the ecliptic plane and three dimensions when the number of crossings per unit direction is variable. In particular, the orientation of the model surface can be very sensitive to the nature of the coverage. For these reasons the assumption of axial symmetry is especially appropriate for comparative investigations, such as this one, given the paucity of observations available at Mars. Further, we will limited ourselves in this study to modeling shock crossings forward of approximately one obstacle radius behind the terminator plane at each planet: Venus $x' > -1R_v$, earth $x' > -10R_e$ and Mars $x' > -1R_{MS}$. Besides avoiding the more poorly sampled downstream regions, this requirement also has the effect of constraining us to that portion of the bow shock which is influenced most by the boundary conditions at the dayside obstacle [e.g., see *Spreiter et al.*, 1966] as will be addressed in part 2, which is concerned more with the solar wind interactions.

The optimum fit to the data on shock position in terms of producing the minimum rms (i.e., "root-mean-square") deviation normal to the model surface would most certainly be a representation in terms of some complete polynomial set with an infinite number of coefficients to be determined (e.g., see the ionopause model of *Theis et al.* [1980a]). However, in terms of usefulness, particularly if any extrapolations are to be made or if the coverage is nonuniform, the objective is to use as few free parameters as is necessary to produce a fit with the requisite accuracy. As a straight line is a very bad representation of shock shape over any substantial length, the standard practice is to use a general second order curve:

$$k_1y^2 + k_2xy + k_3x^2 + k_4y + k_5x + k_6 = 0 \tag{2}$$

Some methods of fitting to this curve are discussed in both *Fairfield* [1971] and *Formisano* [1979], who also includes a z^2 term, with their results listed in Table 3. In considering the nature of the solutions to this equation it must be noted that the k_2 term represents a rotation of the symmetry axes of the solutions (i.e., circles, ellipses, parabolas, and hyperbolas, if we ignore the degenerate cases) about their center by an amount

$$\lambda = 1/2 \tan^{-1}[k_2/(k_3 - k_1)] \tag{3}$$

from a configuration in which the symmetry axes parallel the coordinate axes. Since we are aberrating the crossing locations before fitting and have found no large asymmetries, we can assume $\lambda = \alpha$, the tilt due to the aberration. Rotating the axes by the amount given in equation (2) eliminates the cross term so that we can then have

$$k_1'y'^2 + k_3'x'^2 + k_4'y' + k_5'x' + k_6' = 0 \tag{4}$$

where

$$\begin{aligned} k_1' &= k_3\sin^2\alpha - k_2\sin\alpha\cos\alpha + k_1\cos^2\alpha \\ k_2' &= k_2(1 - 2\sin^2\alpha) + 2(k_1 - k_3)\sin\alpha\cos\alpha \equiv 0 \\ k_3' &= k_3\cos^2\alpha - k_2\cos\alpha\sin\alpha + k_1\sin^2\alpha \\ k_4' &= -k_5\sin\alpha + k_4\cos\alpha \\ k_5' &= k_5\cos\alpha + k_4\sin\alpha \\ k_6' &= k_6 \end{aligned} \tag{5}$$

Equation (4) can then be arranged into a more familiar form

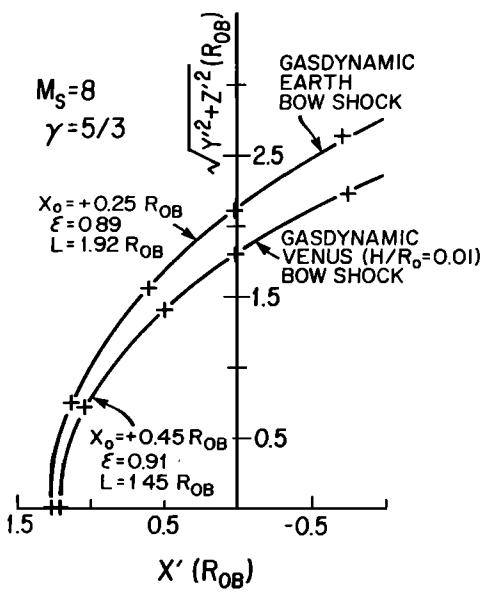

Fig. 5. Best fits to the forward portions of the gasdynamic bow shock models of *Spreiter et al.* [1966] and *Spreiter and Stahara* [1980] are displayed. If downstream data were included the resulting curves would be hyperboloid, but at the expense of the goodness of fit along the forward section.

TABLE 4. Earth Bow Shock Models (Conic Form)

Study	Symmetry Assumption	Domain	λ	x_0, R_e	y_0, R_e	ϵ	L, R_e	Conic Type	α
Fairfield [1971]									
'Meridian 4°'	Spherical ($x' > 0$) Axial WRT x' ($x' < 0$)	$x > -45R_e$	−0.8°	+3.4	+0.3	1.02	22.3	Hyperbola	$\equiv -4.0°$
'Meridian, NO 4°'	Same	Same	−5.2°	+1.5	+0.4	1.07	27.2	Same	$\equiv 0°$
'X ROT., NO 4°'	Axial WRT x	Same	−5.6°	+1.2	−0.1	1.07	27.2	Same	$\equiv 0°$
Formisano [1979] (With $z = 0$)									
'P_{sw} Unnormalized'	WRT Ecliptic ($z = \|z\|$)	Same	−3.6°	+2.6	+1.1	0.97	22.8	Ellipse	$\equiv 0°$
'P_{sw} Normalized'	Same	Same	−9.1°	−4.1	−1.6	0.76	28.1	Same	$\equiv 0°$
This Study									
Imp 3	Axial WRT x'	$x > -10R_e$	$\equiv 0°$	+3	$\equiv 0$	1.19	23.1	Hyperbola	$\tan^{-1}(V_e/V_{sw})$
Imp 4	Same	Same	$\equiv 0°$	+3	$\equiv 0$	1.15	23.5	Same	Same
Heos 1	Same	Same	$\equiv 0°$	+3	$\equiv 0$	1.10	23.5	Same	Same
Pognoz 1,2	Same	Same	$\equiv 0°$	+3	$\equiv 0$	1.20 (±3%)	22.9 (±1%)	Same	Same
Mean #6–9	Same	Same	$\equiv 0°$	+3	$\equiv 0$	1.16	23.3	Same	Same

Equations (2)–(6) have been used to transform the coefficients in Table 3 into geometric quantities for comparison with the results of this study. Alternatively, the results of this work could have been expressed in the same form as used by Fairfield and Formisano, but the terms above are both more insightful and allow for greater ease in use by avoiding the need to solve second-order equations as must be done in the Cartesian form.

$$\frac{(x' + k_5'/2k_3')^2}{(k_4'^2/4k_1'k_3') + (k_5'^2/4k_3'^2) - (k_6'/k_3')} + \frac{(y' + k_4'/2k_1')^2}{(k_4'^2/4k_1'^2) + (k_5'^2/4k_1'k_3') - (k_6'/k_1')} = 1 \quad (6)$$

Finally, this expression can be put into a convenient polar form

$$r = L/(1 + \epsilon \cos \theta) \quad (7)$$

where the semi-latus rectum, $L = b^2/a$, and the eccentricity, $\epsilon = c/a$, are determined from $a = |(k_4'^2/4k_1'k_3') + (k_5'^2/4k_3'^2) - (k_6'/k_3')|^{1/2}$, $b = |(k_4'^2/4k_1'^2) + (k_5'^2/4_1'k_3') - (k_6'/k_1')|^{1/2}$, and $c^2 = a^2 \pm b^2$ (plus sign for a hyperbola and a minus sign for an elipse) with the focus about which (r, θ) are measured located at the point $x_0 = (-k_5'/2k_3') \pm c$, $y_0 = (-k_4'/2k_1')$ where the plus sign is for an ellipse and the minus sign is taken for a hyperbola. Thus so long as the location of the foci are arbitrary, equation (7) is equivalent to (1) with 5 free parameters each. By assuming axial symmetry about the x' axis, two free parameters are removed to leave the eccentricity ϵ, the semi-latus rectum L, and the position of the focus along the x' axis x_0. Thus for this model, three coefficients are determined by fitting the data. As demonstrated by *Slavin et al.* [1980], allowing the location of the focus on the x' axis to be a free parameter results in better fits over the original 2 parameter ϵ–L models of *Holzer et al.* [1966, 1972]. This slight generalization is of particular advantage in this work where the shapes of three different planetary bow waves are being compared. Equation (7) may be rearranged so that

$$\frac{1}{r} = \frac{\epsilon}{L}\cos\theta + \frac{1}{L} \quad (8)$$

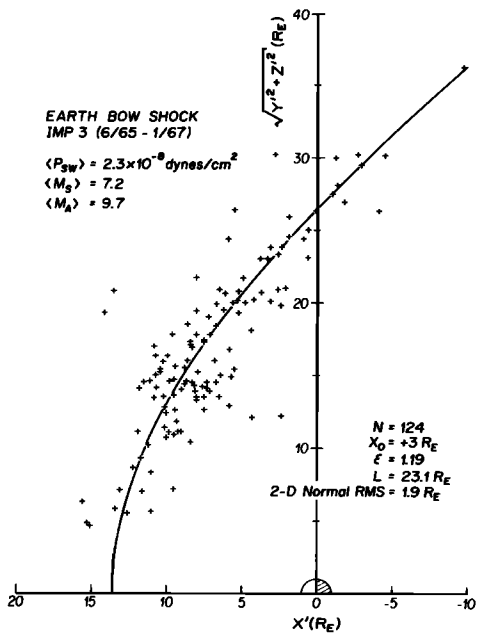

Fig. 6. Three parameter second-order fit to the Imp 3 shock crossings.

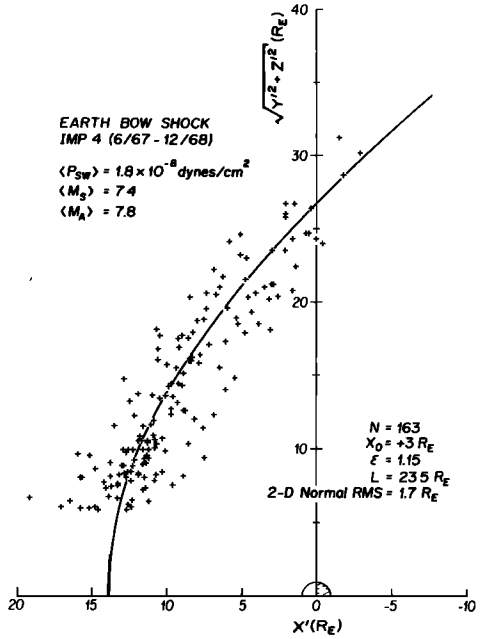

Fig. 7. Three parameter second-order fit to the Imp 4 shock crossings.

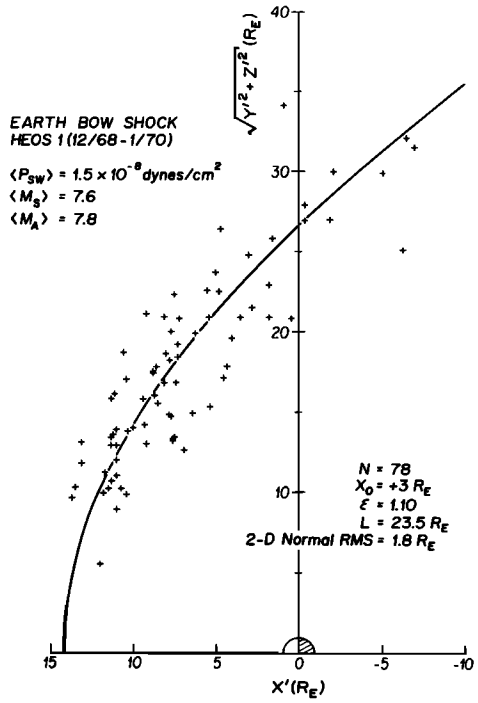

Fig. 8. Three parameter second-order fit to the Heos 1 shock crossings.

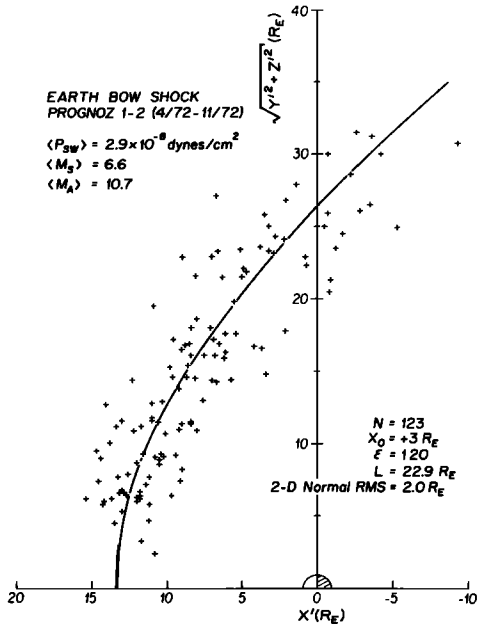

Fig. 9. Three parameter second-order fit to the Prognoz 1 and 2 shock crossings.

and linear regressions in $1/r - \cos\theta$ space performed for different focus locations to identify the fit for which the rms deviation normal to the model surface in the $x' - (y'^2 + z'^2)^{1/2}$ plane is least.

This method is illustrated in Figures 4 and 5 where it has been tested by fitting six points taken off the *Spreiter et al.* [1966] and *Spreiter and Stahara* [1980*b*] gasdynamic models of shock location at the earth and Venus, respectively. In Figure 4 the best fit for the earth model in "conic coordinates" (i.e., conics are all straight lines in $1/r - \cos\theta$ plane) is displayed while Figure 5 shows the results of the exercise in $x' - (y'^2 + z'^2)^{1/2}$ coordinates. Based upon the observed goodness of fit in these two 'test' cases, and past experience [*Slavin et al.*, 1980], we have concluded that the proposed three parameter fitting method will fulfill its intended purpose of modeling the bow waves in the solar wind associated with differing obstacle shapes. Finally, the coefficients of the second order models of Fairfield and Formisano have been expressed via equations (2)–(6) in terms of more geometrically meaningful quantities such as focus location, eccentricity, and semi-latus rectum, which are shown in Table 4. In the sections to follow these models and others will be compared with the results obtained by this study using the 3 parameter second order method described above.

MODELING RESULTS

Earth

As was mentioned in the introduction a series of earth orbiting satellites active during solar cycle 20 (see Figure 3) were selected for use in examining the terrestrial bow wave in order to note any solar cycle effects which might influence the position of the shock. Imp 3 and 4 (D.H. Fairfield and NSSDC, private communication, 1978), Heos 1 (V.V. Formisano, private communication, 1980), and Prognoz 1 and 2 (O.L. Vaisberg and V.N. Smirnov, private communication, 1980) bow shock crossings were obtained, aberrated, and modeled by the three parameter method described previously with the results displayed in Table 4 and Figures 6–9. Table 5 provides a listing of the number of passes, mean upstream conditions [*King*, 1977], and other information pertaining to each data set. The individual satellite observations were fitted separately except in the case of Prognoz 1 and 2, which overlapped in time and were modeled together. With the interval of time during which each satellite provided information being only 6–18 months, no large rapid changes in mean solar wind parameters were found during the individual missions that could bias the results. Such problems would arise if, for example, the subsolar crossings took place during a period of significantly different Mach number, or dynamic pres-

TABLE 5. Earth Bow Shock Data Set

Satellite	#Passes	$\langle P_{sw}\rangle$, dynes/cm²	N	$\langle M_s\rangle$	N	$\langle M_A\rangle$	N	$\langle M_{MS\perp}\rangle$	$\langle M_{MS\parallel}\rangle$	N	R_{ss}, R_e
Imp 3	124	2.3×10^{-8}	57	7.2	57	9.7	48	5.6	6.9	48	13.5 ± 0.3
Imp 4	163	1.8×10^{-8}	86	7.4	86	7.8	76	4.9	6.3	76	13.9 ± 0.3
Heos 1	78	1.5×10^{-8}	70	7.6	32	7.8	49	4.8	6.1	21	14.2 ± 0.3
Prognoz 1,2	123	2.9×10^{-8}	37	6.6	37	10.7	36	5.4	6.4	36	13.4 ± 0.3
Total (Mean)	488	(2.1×10^{-8})	250	(7.2)	212	(9.0)	209	(5.2)	(6.4)	181	(13.8)

Average upstream parameters have been tabulated, including the average dynamic pressure and the Alfvénic, sonic, and magnetosonic Mach numbers. The sonic Mach numbers were computed as in Table 2 but with an assumed T_e of 1.5×10^5 °K. In each case, the number, N of instances in which hourly averaged upstream parameters [*King*, 1977] were available is also listed. Note the relatively small number of cases (i.e., <50%) in which Mach numbers may be calculated even when hourly averages are utilized. The distance to the nose of the bow wave R_{ss} varies monotonically with P_{sw}, but there are significant contributions from solar wind Mach numbers as may be seen in Figure 10.

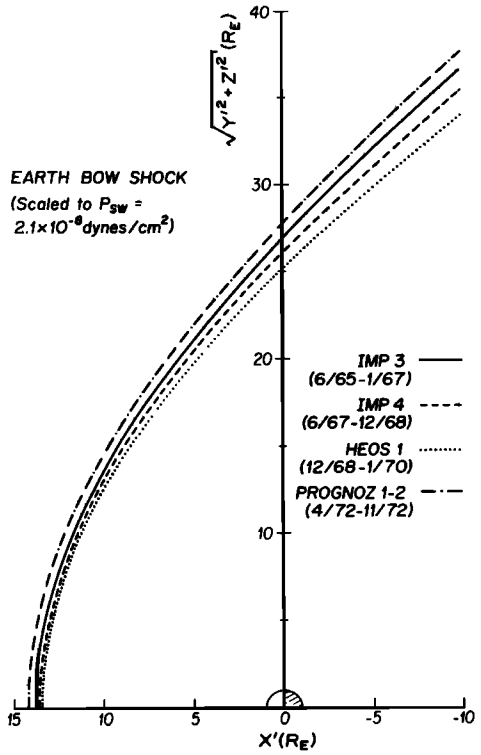

Fig. 10. Earth bow shock models from Imp 3, Imp 4, Heos 1, and Prognoz 1–2 all scaled to the mean solar wind dynamic pressure are displayed.

sure, conditions from those present when the flank observations were made. This difficulty may be avoided altogether by selecting data on the basis of interplanetary conditions, but sufficient measurements to conduct such a study do not exist for Mars and are only just becoming available at Venus [see *Slavin et al.*, 1980]. Since for the sake of comparison it is desirable to analyze the earth bow wave in the same manner as at the other planets, we have modeled separately the average terrestrial bow wave observed by each mission as opposed to using a single merged data set.

The sampling of the boundary surface is quite good between ~ 20° and ~ 95° in sun-planet-satellite angle. Few subsolar observations are available owing to the generally nonequatorial latitudes of satellite apogees and the assumption of axial symmetry as opposed to, for example, spherical symmetry [e.g., *Fairfield*, 1971]. The least sensitive of the model parameters was the focus location x_0. In each case the best fits were obtained for $x_0 = +3\ R_e$, but with only slightly poorer representations at +3.5 and +2.5 R_e. This finding is similar to the 'meridian 4°' model of *Fairfield* [1981] listed in Table 4, which shows an x_0 value of +3.4 R_e when a 4° aberration is assumed before fitting the data. However, there is a large variation in x_0 from +2.6 to −4.1 R_e *in the Formisano* [1979] model when the data are scaled by $P_{sw}^{1/6}$ to take into account the dependence of magnetopause radius on upstream dynamic pressure. For a given focus location in our study significant degradation in the goodness of fit is observed with changes from the optimum in the eccentricity ϵ, and semi-latus rectum L, at the ~ 3% and ~ 1% levels, respectively, as indicated in Table 4. In each case the type of second order curve obtained was a hyperbola with the eccentricities ranging from 1.10 for Heos 1 to 1.20 for Prognoz. These results compared favorably with the 1.02–1.07 values from the Fairfield study. The Formisano model also produced a similar result, $\epsilon = 0.97$, when no scaling for varying P_{sw} was included. However, the normalized model with $x_0 = -4.1\ R_e$ found a far more elliptical shock surface of eccentricity 0.76. The possible reasons for the similarity among the ϵ and x_0 values obtained here and the P_{sw} unnormalized models of Fairfield and Formisano, as contrasted with the Formisano normalized case, will be considered in the discussion section. Finally, the two dimensional rms deviation normal to the model surfaces in Figures 6–9 are relatively constant with a maximum of 2.0 R_e for Prognoz 1–2, and a minimum of 1.7 R_e for Imp 4.

The bow shock stand-off distance along the x' axis

$$R_{ss} = x_0 + \frac{L}{1+\epsilon} \tag{8}$$

is tabulated in Table 5 and shown to vary monotonically with the highest dynamic pressure, which occurs before and after solar maximum, producing the minimum R_{ss} and the lowest dynamic pressure, near solar maximum, associated with the largest R_{ss}. Figure 10 shows the 4 model shocks scaled (i.e., scaling both x_0 and L) to the mean pressure by assuming a $P_{sw}^{1/6}$ magnetopause pressure dependence [e.g., *Holzer and Slavin*, 1978]. As will be examined in part 2 of this study, both the stand-off distance and shock shape (i.e., for x_0 constant, the eccentricity) for the bow wave models in Figure 10 appear ordered by the average sonic Mach numbers in Table 6 with the highest $<M_s>$, 7.6 for Heos 1, producing the most slender shock and thinnest magnetosheath. By comparison,

TABLE 6. Summary of Principal Second Order Venus Bow Shock Models (Conic Form)

	Study	S/C	Period	#Passes	Symmetry Assumption	Domain	λ	$x_0(R_V)$	$y_0(R_V)$	ϵ	$L(R_V)$	Conic Type	α
1.	Slavin *et al.* [1979*a*]	PVO	1978–9	86	Axial WRT x'	$x' > -1R_V$	≡0	≡0	≡0	0.80	2.44	Ellipse	$\tan^{-1}\left(\frac{V_V}{V_{sw}}\right)$
2.	*Slavin et al.* [1980]	PVO	1978–9	172	Axial WRT x'	$x' > -1R_V$	≡0	+0.2	≡0	0.88 (±4%)	2.21 (±0.5%)	Ellipse	Same
3.	*Smirnov et al.* [1980]	V9-10	1975–6	45–62	Axial WRT x'	$x' > -16R_V$	≡0	+0.41	≡0	1.04	1.70	Hyperbola	Same
		PVO	1978–9	86	Same	$x' > -1R_V$		=0	≡0	0.80	2.44	Ellipse	Same
		PVO	Same	86	Same	Same	≡0	+0.29	≡0	1.02	2.17	Hyperbola	Same
4.	This study	V9-10	1975–6	48	Axial WRT x'	$x' > -1R_V$	≡0	+0.2	≡0	0.89 (±3%)	1.95 (±1%)	Ellipse	Same
5.	Mean of 2 and 4 (Solar Cycle average?)	•••	•••	•••	•••	$x' > -1R_V$	≡0	+0.2	≡0	0.89	2.08	Ellipse	

As a result of the large number of bow shock observations at Venus which have been made over the last five years much progress has taken place in the modeling of this boundary. For this reason the earlier model surfaces based upon a small numberof shock encounters [e.g., *Russell*, 1977] have not been listed above.

Prognoz 1–2 with $\langle M_s \rangle = 6.6$ gave the bluntest bow wave and thickest magnetosheath. This results is in qualitative agreement with the expectations of both the available gasdynamic [e.g., *Spreiter et al.*, 1966] and MHD [*Spreiter and Rizzi*, 1974] theoretical models in the limit of the large Alfvenic Mach number (i.e., $M_A^2 = Q = \frac{1}{2}nmV_{sw}^2/(B^2/8\pi) > 10^2$). Magnetosonic Mach numbers are often invoked in the studies of the near shock on intuitive grounds, contrary to the results of the existing MHD models [*Spreiter and Rizzi*, 1974; *Chao and Wiskerchen*, 1974]. Inspection of Table 5 and Figure 10 shows them to be uncorrelated to the location and shape of the near shock to within the resolution of this study. However, this should not be taken to imply that far downstream the position of the shock is not being limited by the value of the fast model MHD wave speed. Eventually, the bow wave is indeed expected to weaken and decay as it approaches the fast wave Mach cone [*Michel*, 1965; *Dryer and Heckman*, 1967]. This behavior has in fact been observed at Venus, the earth, the Moon, and Mars [e.g., *Whang and Ness, 1970; Bavassano et al., 1971; Bogdanov and Vaisberg*, 1975; *Slavin and Holzer*, 1981]. But it must be remembered that forward of the obstacle the shock is still strong with its shape and position determined by the need to deflect the flow about the planet while conserving mass, momentum, and energy. The concept of 'Mach Cone' based upon a MHD signal speed which is useful far downstream has no physical validity in the forward regions as can be seen, for example, by consideration of the magnetosheath flow characteristics discussed by *Spreiter et al.* [1966].

Venus

As treated in the recent reviews by *Breus* [1979], *Russell* [1979] and *Siscoe and Slavin* [1979] Venus bow shock crossings were recorded by a number of the early (i.e. and 1961–74) Venera and Mariner spacecraft flights culminating with the Venera 9 and 10 and Pioneer Venus orbiter missions of 1975–6 and 1978, respectively. The trajectories of these three satellites differ most in that the V9-10 orbital planes were only moderately inclined, ~30°, to the ecliptic with periapsis altitudes in the 1500- to 1600-km range while that of PVO is highly inclined, ~106°, with a periapsis in the ionosphere at heights as low as ~140 km. Table 6 summarizes the Venus bow shock models by using second order curves resulting from these orbiter mission observations. In a preliminary Pioneer Venus study with the focus assumed coincident with the center of the planet (i.e., $x_0 \equiv 0$), *Slavin et al.* [1979*a*] found an eccentricity of 0.80 and a semi-latus rectum of 2.44 R_v. This result was reproduced by *Smirnov et al.* [1980] utilizing similar methods and the same set of crossings. With the focus allowed to move along the x' axis as in this study, *Slavin et al.* [1980], using twice the number of points, 172, as the earlier study, determined a best fit of $x_0 = +0.2\,R_v$, $\epsilon = 0.88$, and $L = 2.21\,R_v$ with an rms deviation normal to the model surface of $0.16\,R_v$. From the original 86 crossings of the *Slavin et al.* [1979] work, Smirnov et al. obtained values of $x_0 = +0.29\,R_v$, $\epsilon = 1.02$, and $L = 2.17\,R_v$ when focus position was added as a third free parameter. Part of the difference between these two x_0–ϵ–L models of the PVO data is undoubtedly the different data sets that were studied, but there may also be differences in the criteria used in determining the 'best' fit. An examination of the Venera 9 and 10 (O.L. Vaisberg and V.N. Smirnov, private communication, 1979) was conducted for $x' > -1\,R_v$, using the same method as applied to the earth in Figures 6–9 in the PVO model of *Slavin et al.* [1980] with the results shown in Figures 11 and 12. The shapes of the near planet bow wave obtained in this way for Venera and PVO are nearly identical in focus location and eccentricity, but with a ~13% increase in semi-latus rectum between the 1975–6 and 1978–9 observations. As discussed in *Slavin et al.* [1979*b*, 1980] such a large variation cannot be explained by the small observed variations in ionopause height. In addition, both the published in situ solar wind observations and the downstream Venus shock location at solar minimum and maximum show no variation in Mach number which could produce such a large growth in shock stand-off distance. This view is supported by Figure 10, which shows the terrestrial bow shock to have been about 5% closer to the magnetopause near solar maximum than before or after that epoch. The implications for such a change of shock location in terms of the solar wind interaction with Venus will be examined in part 2 of this study.

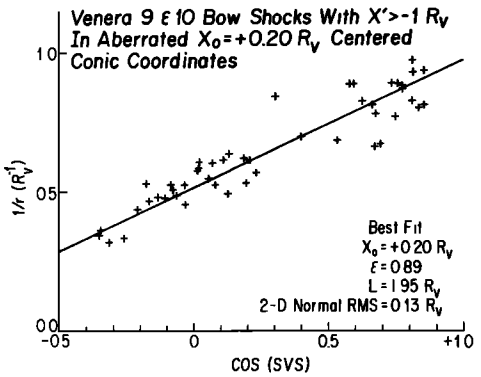

Fig. 11 Three parameter second-order fit to the Venera 9 and 10 shock crossings at Venus in the $1/r$ – cos θ plane.

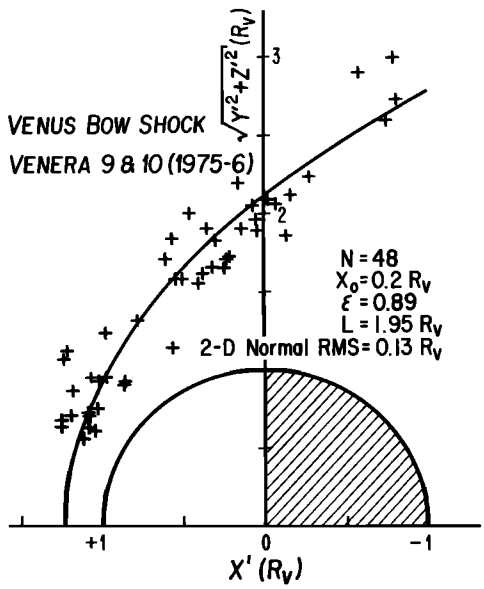

Fig. 12. Best fit to the Venera 9 and 10 shock observations from preceding figure displayed in aberrated solar ecliptic coordinates centered on Venus.

Figure 13 further considers the question of a solar cycle dependence in the Venus bow wave position by plotting the four shock models appearing in Table 6, and discussed above, along with that of *Verigin et al.* [1978]. The Venera 9 and 10 shock crossings of Smirnov et al., a subset of which were used in this study, came from the RIEP plasma spectrometer observations [*Vaisberg et al.*, 1976]. *Verigin et al.* [1978] have published a set of shock crossings based upon the wide-angle plasma analyzers measurements (i.e., a modulated Faraday cup, *Gringauz et al.* [1976] which are shown in Figure 13 as solid line segments over the portions of the Venera trajectory during which the transition between shocked and unshocked solar

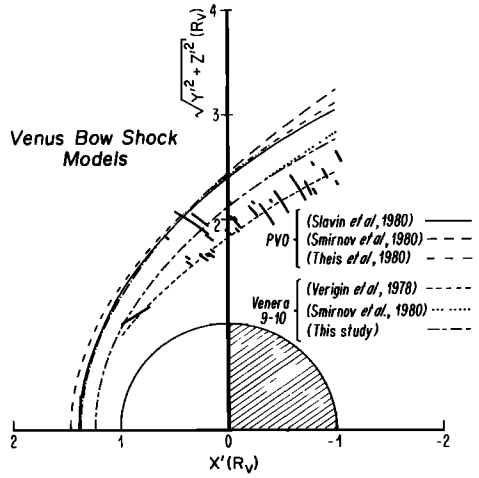

Fig. 13. Venus bow shock models derived from Venera 9 and 10 and Pioneer Venus shock observations are displayed along with the bow wave crossings of *Verigin et al.* [1978].

wind took place (note: The Verigin et al. crossings have not been aberrated. However, if similar numbers of dawn and dusk hemisphere crossings were included, then the effect is just to increase the width of the distribution in Figure 13. See *Gringauz* [1980]). The dashed curve in that figure is a gasdynamic shock that Verigin et al. passed through their crossings. It is at once apparent that although the Smirnov et al. Venera orbiter model and ours show agreement, the mean curve and individual shock positions of Verigin et al. lie somewhat closer to the planet. This is especially troublesome as both Smirnov et al. and Verigin et al. claim good agreement with the magnetometer experiment [*Dolginov et al.*, 1976] as to the location of the bow wave. The reason may then be one of data selection in these studies, but only a careful comparison of their measurements could reveal it. However, regardless of this unexplained discrepancy it is clear in both data sets that the position of the bow shock was indeed closer to Venus during the epoch of Venera 9 and 10 than that of PVO.

Also shown in Figure 13 are all three models of the Venus shock based upon PVO data that have been published thus far. Those of *Slavin et al.* [1980] and *Smirnov et al.* [1980] were discussed earlier and show very similar results. The third, by *Theis et al.* [1980b], employs a novel approach in that it uses a polar curve which they term an 'Archimedian Hyperboloid' formed from the sum of hyperbolic and Archimedian spirals. This two free parameter model is seen to predict shock locations similar to those of the other two but with the subsolar point somewhat more distant. This latter difference may be due in part to not only the spiral shape assumed in their two-parameter fit, but also the lack of any data selection in that study. *Slavin et al.* [1979*a*, 1980] omitted crossings in certain regions to limit biasing of the representation by the orbit of Pioneer Venus paralleling the shock surface at smaller sun-planet-satellite angles. In general, the use of any reasonable prescribed shape such as spirals is little different than assuming, for example, that the shock surface is paraboloid [e.g., *Egidi et al.*, 1970]. Many different types of curves exist which may be used unless it is desired to actually determine the shape of the bow wave as is the case in this work and a few of the other studies [e.g., *Fairfield*, 1971; *Russell*, 1977; *Formisano*, 1979]. To do this, the model surface shape must be variable with at least, in our experience, three free parameters to fit the observed variation among the planet's bow waves. The model of Theis et al. demonstrates graphically the lack of any uniqueness in the frequently used model formulations that assume the shape of the shock surface prior to fitting the measurements.

Mars

Although the Red Planet has been the subject of an intensive research effort by both the U.S. and U.S.S.R. over the past two decades, including six orbiter missions, less is known about the particles and fields environment of Mars than any of the other planets probed thus far. The reason is that only Mariner 4 fly-by and the Mars 2, 3, and 5 orbiters were instrumented to cary out such measurements near Mars, and even then no data were obtained at low altitudes, beneath $\sim 10^3$ km, or deep in the wake region [*Vaisberg et al.*, 1976; *Dolginov et al.*, 1976; *Gringauz et al.*, 1976]. More specifically, it has long been known that Mars deflects the solar wind, as opposed to absorbing it like our moon, because of the strong bow shock detected by Mariner 4 (see Figure 1). However, it has not been possible to identify unambiguously the processes by which the flow is diverted in the absence of low altitude observations [e.g., *Russell*, 1978*a*,*b*; *Dolginov*, 1978*a*,*b*]. For the purpose of modeling the Martian bow wave a set of boundary crossings identified by the Mars 2, 3, and 5 RIEP plasma instruments (O.L. Vaisberg and V.N. Smirnov, private communication, 1979) in general agreement with the other experiments [*Vaisberg*, 1976] were obtained. In Figure 14 the average crossing location per pass is modeled with the three parameter fit used previously on the Earth and Venus data. Figure 15 displays both the model and the intervals over which the transition between shocked and unshocked solar wind took place a long the individual satellite trajectories. In one case, several multiple encounters by Mars 3 are connected by dashed lines to avoid attributing them to three separate passes and weighing them more heavily. The remote crossing labeling 'A' was not included in the fitting although its presence, when allowed, did not cause any large changes in the best fit parameters. In Part 2, this crossing and one other just downstream of the $x' = -1\ R_{ms}$ plane (also marked with 'A' in Figure 17) are modeled as low Mach number events. This possibility was first suggested by *Vaisberg* [1976]. Accordingly, their usually larger distances from the planet may not be so indicative of the solar wind interaction being unusual on those occasions as the upstream conditions being atypical (e.g., low M_s). Despite the limited nature of the coverage, the shock location does appear to be adequately sampled, particularly in terms of SMS angle, by these three orbiter missions, and there is reason to have confidence in the results. Sources of spatial biasing by the spacecraft trajectories will be discussed below.

Listed in Table 7 and plotted in Figure 16 are a number of different models of the Mars bow shock. Both *Bogdanov and Vaisberg* [1975] and *Russell* [1977] used the ϵ–L shock modeling method of *Holzer et al.* [1966, 1972] to fit different sets of orbiter shock crossings, but produced different mean surfaces due to their

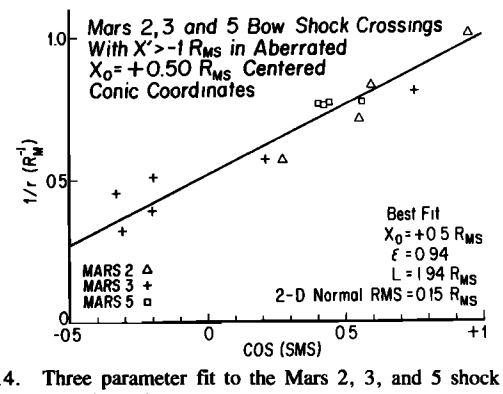

Fig. 14. Three parameter fit to the Mars 2, 3, and 5 shock crossings forward of the plane $x' = -1R_{MS}$.

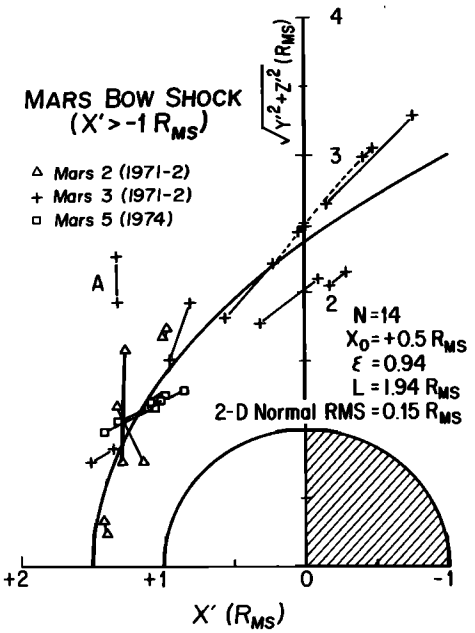

Fig. 15. Best fit to the Mars bow shock crossings from the preceding figure displayed in aberrated solar ecliptic coordinates centered on Mars. The shock crossing marked 'A' has not been considered in obtaining the fit, but only minor modifications result when it is included.

different data sets. The *Gringauz et al.* [1975] and *Gringauz* [1975] curves are previously published gasdynamic models scaled to their observations (i.e., one free parameter) and as such are not very sensitive to the actual observational data in terms of determining the shape of the bow waves. In comparing these models, the most significant difference is that the shock surface obtained in this study is seen to be much less blunt than those obtained in the other works. The reason appears to be less the nature of the modeling technique than the set of crossings utilized. In Figure 17 we have plotted all of the Mars 2, 3, and 5 shock crossings along with some representative orbital paths. First, it is apparent that by limiting the study to those crossings forward of $-1\,R_{MS}$ we do not include two crossings just anti-sunward of this plane at least one of which is much farther from the x' axis than is consistent with typical Mach number conditions and the shock observations farther downstream. In Part 2 the two crossings marked 'A' in Figure 17 are both modeled as a single low Mach number event given that the difference in time between these Mars 2 and Mars 3 crossings was only about 7 hours. In addition, the two Mars 3 bow wave crossings closest to the planet in the vicinity of the aberrated terminator plane are absent from all of the studies cited save the one by *Bogdanov and Vaisberg* [1975]. Thus, we find that blunter bow wave models obtained by most of the previous studies are due largely to the inclusion of the two crossings just anti-sunward of $x = -1\,R_{MS}$. Shock crossings may be recorded only along the paths of the available spacecraft. In this case the very limited nature of the Mars 2 and 3 spatial coverage downstream of the terminator, as shown in Figure 17, has led to the other models tending to produce shock surfaces which follow the orbits of these satellites. The Mars 5 bow wave encounters near $x' - 5\,R_{MS}$ from a trajectory which is less parallel to the boundary clearly support the more slender shock model we have arrived at after data selection.

Testing Axial Symmetry

By comparison with the two and three dimensional 2nd order models of *Fairfield* [1971] and *Formisano* [1979], we have removed 2 and 3 free parameters, respectively, with the assumption of axial symmetry about the x' axis. These studies do lend support to this assumption that in y_0, the y coordinate of focus position after the conic has been rotated by the angle λ, tends to be small and much less is absolute magnitude than x_0 as shown in Table 4. Further, the models of Fairfield find only 0.8° and 0.6° tilt beyond the mean aberration angle (i.e., $\lambda = \tan^{-1}(30/430) = 4°$), while the models of Formisano give much more, $\lambda = 9.1°$, or slightly less, $\lambda = 3.6°$, than expected for aberration depending upon whether or not a scaling factor for solar wind dynamic pressure is added. As was discussed earlier, the addition of the solar wind dynamic pressure scaling into the Formisano model brings about large changes in the shock model surface that conflict with the results of *Fairfield* [1971] and this study. In the next section we will present arguments to the effect that these anomalous results are an artifact due to the modeling method employed in that study vis-à-vis the $\sim 10^3$ Heos 2 multiple shock encounters included in his shock data set.

The theoretical expectation of a lack of axial symmetry originates with the observational fact that the interplanetary magnetic field is only rarely aligned with the solar wind velocity vector. In this event **B** and **V** would remain parallel in the magnetosheath due to the 'frozen flux' condition (barring interactions with the geomagnetic field and non-MHD processes) and yield an axially symmetric flow. For all other IMF orientations, such as the average

TABLE 7. Mars Bow Shock Models

Study	S/C	Period	#	Symmetry Assumption	Domain	λ	$x_0(R_{MS})$	$y_0(R_{MS})$	ϵ	$L(R_{MS})$	Conic Type	α
Bogdanov and Vaisberg [1975]	Mariner 4	7/15/65	2	Axial WRT x	$x > -13R_{MS}$	$\equiv 0$	$\equiv 0$	$\equiv 0$	1.08 (±32%)	2.83 (±4%)	Hyp.	=0°
	Mars 2	1971-2	7									
	Mars 3	Same	9									
		(total	18)									
Russell [1977]	Mars 2	1971–2	3	Axial WRT x	$x > -3R_{MS}$	$\equiv 0°$	0	$\equiv 0$	0.99 (±11%)	3.00 (±4%)	Ell.	=0°
	Mars 3	1971–2	4									
	Mars 5	1974	4									
		(total	11)									
This study	Mars 2	1971–2	4	Axial WRT x'	$x' > -1R_{MS}$	$\equiv 0°$	+0.5	$\equiv 0$	0.94 (±4%)	1.94 (±1%)	Ell.	$\tan^{-1}\left(\frac{V_{MS}}{V_{sw}}\right)$
	Mars 3	1971–2	6									
	Mars 5	1974	4									
		(total	14)									

The degree to which the solar wind interaction ith Mars has been ignored in the planning of missions is very apparent in the small number of shock observations recorded above. The 1965 Mariner 4 fly-by represents the entire American contribution. According, fewer quantitative modeling efforts have been aimed at the Mars shock surface.

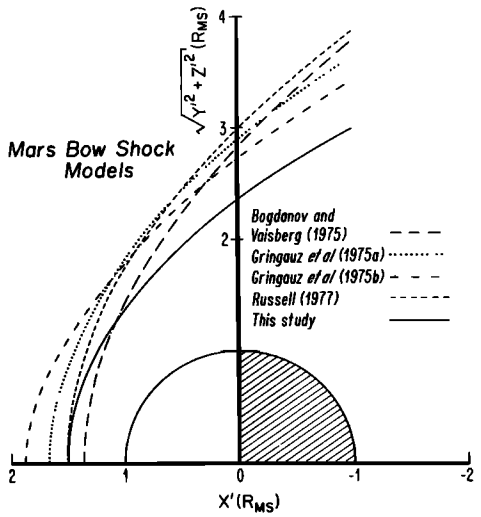

Fig. 16. Mars bow shock models derived from the Mars 2, 3, and 5 observations with the one from this study being most different due to its consideration of only the better sampled forward region (i.e., $x' > -1R_{MS}$).

Parker spiral configuration, draping of the field lines produces magnetic stresses possessing symmetry only with respect to a plane containing the x' axis and parallel to the magnetic field. Unfortunately, the only complete MHD flow model of the magnetosheath is that of *Spreiter and Rizzi* [1974] for aligned **B** and **V**, which is accordingly axisymmetric about x'. *Walters* [1964] examined the MHD jump conditions across the bow shock in 2 dimensions and noted that the spiral orientation of the IMF caused the apparent stagnation point (i.e., the location on the shock surface where flow crossing the shock is slowed, but not deflected) to shift from coincidence with the x' axis by an amount dependent upon the upstream β, Q, and the IMF direction with respect to solar wind velocity and the shock surface. For a Parker spiral IMF with $\beta = 0.5$ and $Q = 40$ (i.e., $M_A = \sqrt{40} = 6.3$) he found a 7.5° tilt in the same direction as, but in addition to, the effects of aberration. However, as can be seen in Tables 1, 2, and 5 more typical values would be $\beta \sim 1-2$ and $Q \sim 90-100$. Hence the choice of mean parameters by Walters based upon the limited interplanetary measurements of his day significantly over estimated the relative strength of the IMF. When these mean parameters are coupled with the actual large variability of the IMF about the Parker spiral, it is not clear that the model of Walters would not in fact, predict only a small additional tilt near ~ 1°. The optimal method of testing this hypothesis with the observations is to select only high interplanetary magnetic field intensity conditions (i.e., low β, M_A) with orientations close to the average spiral for modeling in order to examine only maximum asymmetry conditions. While such an investigation is beyond the scope of this study, the fact remains that Walters' analysis of the jump conditions along the bow wave does not necessarily predict any significant asymmetry in the mean with respect to the natural distribution in upstream parameters. This consideration has apparently been overlooked in previous studies. In addition, the approximate two dimensional MHD flow solutions of *Shen* [1972] suggest that the effect noted by Walters may not result in any net east-west asymmetries in the shock surface due to the restoring stresses of the draped magnetosheath fieldlines. *Zhuang et al.* [1981] in another approximate MHD calculation find only slight (i.e., < 1°) deviations of the equatorial magnetopause symmetry axis from the x' axis. Further, any observational resolution of this fluid problem will be complicated by the influence of collisionless shock structure upon the conservation of momentum and energy across the bow wave. Quasi-parallel structure, for example, can result in some deceleration of the solar wind upstream of the shock through wave-particle interactions in the foreshock region [e.g., *Bonifazi et al.*, 1980], while the enhanced turbulence downstream relative to quasi-perpendicular conditions may act as an additional energy sink and result in a small decrease in local magnetosheath thickness [e.g., *Formisano et al.*, 1973; *Chao and Wiskerchen*, 1974].

We examine the observational validity of the axial symmetry assumption used in this study further in Table 8. Those Imp 3, Imp 4, Heos 1 and Prognoz 1–2 crossings for which measured solar wind speeds were available to transform them into (x', y', z') coordinates have been mapped into the aberrated terminator plane by means of their respective model surfaces (i.e., Table 4). They have been separated by the y' coordinate into dawn and dusk groupings with their mean distances and statistical uncertainties listed in the table. As shown in 3 of the 4 sets of crossings, the difference δ between the mean dusk radius and the mean dawn value is less than the uncertainty. However, in all cases the distance to the shock on the duskside is indeed slightly greater than or equal to that at dawn so that it may be that some slight asymmetry exists on the average which a much larger number of crossings could resolve. Nevertheless, it is clear that the assumption of axial symmetry, and hence our three-parameter modeling method, is valid to within the statistical resolution of the data set.

In addition to the two-dimensional dawn-dusk asymmetry model proposed by *Walters* [1964], *Cloutier* [1976] suggested that deviations from axial symmetry would also occur due to draped configuration of magnetosheath magnetic field lines causing the flow to behave like a fluid with two degrees of freedom (i.e., $\gamma = 2$) in regions where flow velocity is perpendicular to the magnetic field and three degrees of freedom ($\gamma = 5/3$) when flow velocity is aligned with *B. Romanov et al.* [1978] reported evidence for such an asymmetry in their Venera 9 and 10 shock crossings after mapping them into the terminator plane and aligning the component of the interplanetary magnetic field in the $y'-z'$ plane at the time of each crossing with a single direction as shown in Figure 18. They found the trace of the bow wave in the terminator plane, as displayed with

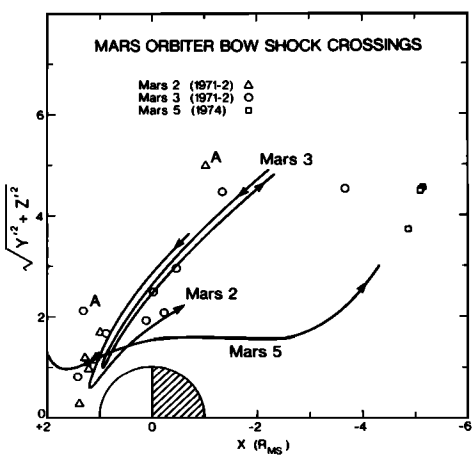

Fig. 17. Mars bow shock crossings (O. L. Vaisberg and V. N. Smirnov, private communication, 1979) displayed along with sample satellite trajectories in January 1972 for Mars 2 and 3 and February 1974 for Mars 5. The downstream Mars 5 bow wave encounters have not been included in any of the models shown in the preceding figure. As a result, there is a strong tendency for all of the empirical surfaces, save the one produced by this study, to be biased outward from the x' axis by the limited spatial coverage of Mars 2 and 3. The crossings marked with the letter 'A' are discussed in the text.

TABLE 8. Dawn-Dusk Asymmetry Search For Earth Bow Shock

S/C	$y' > 0$ (Dusk) N	$y' > 0$ (Dusk) $< r(x' = 0) >$	$y' < 0$ (Dawn) N	$y' < 0$ (Dawn) $< r(x' = 0) >$	$\delta(R_e)$
Imp 3	34	26.3 ± 0.7	28	25.8 ± 0.5	+0.5 ± 0.9
Imp 4	68	27.0 ± 0.3	46	26.0 ± 0.4	+1.0 ± 0.5
Heos 1	27	27.0 ± 0.5	43	26.4 ± 0.7	+0.7 ± 0.9
Prognoz 1,2	22	25.9 ± 0.7	65	25.9 ± 0.4	+0.0 ± 0.8

As described in the text the shock observations have been mapped into the aberrated terminator plane separately for the dawn and dusk hemispheres. While there is some suggestion of asymmetry, any real difference in the distance to the bow shock in these two hemispheres must be less than the statistical uncertainties, $\sim 1\ R_e$.

dashes, to be elliptical in approximate agreement with the predictions of Cloutier. *Slavin et al.* [1979*b*, 1980] repeated this experiment with much larger sets of observations from Pioneer Venus and found the Venus bow shock to be axisymmetric about x' to within the statistical errors shown in Figure 18. By using the Imp 4 bow wave crossings and hourly averaged magnetic field observations, this process was repeated at earth with the same results as displayed in the figure. Thus, again we conclude that our assumption of axial symmetry for this study is valid. In the case of the Romanov et al. finding, the lack of symmetry may be due to the inclusion of shock crossings up to $\sim 8R_v$ downstream of Venus. At such distances the bow wave is beginning to asymptote with the expected result being an elliptical cross section whose eccentricity is determined by the ratio of $M_{MS\|}$ to $M_{MS\perp}$ (i.e., the fast mode Mach numbers parallel and perpendicular to the IMF direction).

DISCUSSION

In the preceding sections three parameter second order bow wave models have been developed for Venus, earth, and Mars and contrasted with existing models. Figure 19 continues this process by displaying the terrestrial bow wave model from this study along with the five-parameter model of Fairfield and the ecliptic plane trace of the six parameter three-dimensional unnormalized model of Formisano. No corrections have been made to allow for diferences between the three models in the mean upstream parameters, such as P_{sw}, that each represent. The Fairfield 'Meridian 4°' model has been used because it was based upon aberrated data while the ecliptic trace of the Formisano unnormalized model has been aberrated by a 3.6° rotation to make it symmetric about a line parallel to the x' axis even though the implied 480 km/s solar wind speed is ~10% higher than expected. The agreement between the three models over the dayside portion of the bow wave is good with the unnormalized model of Formisano and the mean surface from this study bracketing the Fairfield model further downstream. The dawn-dusk asymmetry in the unnormalized Formisano surface is due to the $+1.1\ R_e$ displacement of the focus toward dusk shown in Table 4, while that of the Fairfield model is split between a $+0.3\ R_e$ offset in the focus and a 0.8° tilt beyond the assumed 4° due to aberration. If 4° had been taken as the rotation associated with aberration in the Formisano model, then a 0.4° tilt in a sense opposite to that of Fairfield's model would have resulted. In comparing these curves it should be noted that the downstream regions, in which the effects of any asymmetry in the bow wave are greatest, are only slightly better sampled in the Formisano and Fairfield models which include some Explorer 33 and 35 observations. The present study, as stated previously, terminates at $x' = -10R_e$. However, it is the presence of the observations between $-45\ R_e < x' < -10R_e$ that results in the slightly lower eccentricities of the Fairfield and Formisano models relative to the ones produced by this study. Had we included the downstream observations, our model would not flair out from the x' axis to the degree that it does and would better represent the Explorer 33 and 35 shock encounters at lunar distances. But, by omitting the downstream crossings a superior fit to the near shock surface is obtained which is the declared goal of this modeling exercise.

The model which has not been plotted in Figure 19 is the P_{sw} normalized one of *Formisano* [1979]. As shown in Tables 3 and 4, that study found a very different model surface when they scaled their observations to a common dynamic pressure. Performing such a scaling is, in fact, highly desirable when merging shock crossings from different periods of the solar cycle due to P_{sw} (which has a solar cycle dependence; *Fairfield* [1979]) being the dominant influence on shock position by largely controlling magnetopause altitude (see *Egidi et al.* [1970], *Holzer and Slavin* [1978], and Table 5/Figure 10 of this report). The expectation is that this procedure should decrease the 'noise' (i.e., reduce the rms deviation from the average surface) and allow refinements in the bow wave model. Under these circumstances it might then be possible to resolve lower order effects influencing shock position. However, when Formisano did this, all of the model coefficients changed markedly and the tilt λ increased by over 250%. Given the good agreement between the unnormalized model and the results of the Fairfield study and our own, the inference would then be that the normalized model had in

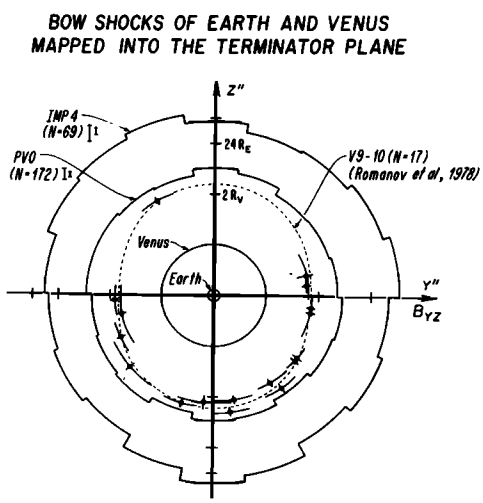

Fig. 18. As described in the text shock crossings by PVO and Imp 4 have been mapped into the aberrated terminator plane and rotated about the x' axis until the component of the IMF in he $Y'-Z'$ plane at the time of the crossing is aligned with the Y' axis. The larger sample error bar in each case refers to the average standard deviation about the mean in each angular sector while the smaller error bar is the average uncertainty of the mean observed for each angular sector. In contrast to the results of *Romanov et al.* [1978] no significant deviations from axial symmetry are apparent in the PVO and Imp observations.

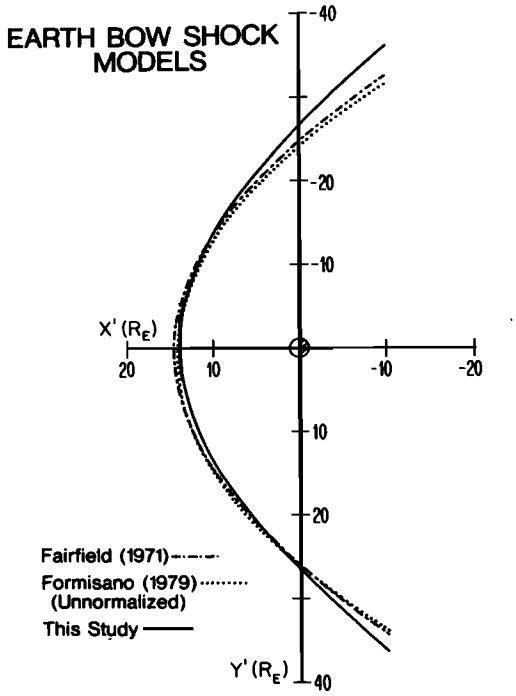

Fig. 19. The mean earth bow shock from this study is compared with the 'unnormalized' model of *Formisano* [1979], which we have rotated by 3.6° to include the suggested effects of aberration, and the 'meridian 4° aberration' model of *Fairfield* [1971], both of which include downstream crossings at lunar orbit.

fact been highly biased by the correction. The probable cause is the large number, $\sim 10^3$, of multiple shock crossings at high latitudes by Heos 2 in the Formisano data set. While these data allow him to model the shock in three dimensions, they do not provide information on the lower latitude shock. At the lower latitudes the data set of Formisano is essentially that of Fairfield with only the addition of Heos 1, a $\sim$ 35% enhancement in the number of crossings. Hence, the ecliptic trace of the three-dimensional model should agree with the two-dimensional models of Fairfield and this study. As shown in Figure 19 and Table 4, this is indeed the situation for the unnormalized Formisano shock surface, but not the normalized model. In fact, judging from the figures in *Formisano* [1979] it appears that the normalization procedure worsens the fit to the data near the ecliptic. It is the Heos 2 portion of the data that appears to be smoothed by the $P_{sw}^{1/6}$ scaling. Thus, we feel there is justification for our suggestion that the Heos 2 high-latitude data, even though it has been weighted, is dominating the Formisano normalized model near the plane of the ecliptic. When more measurements are available from different orbits at high latitudes, it should be possible to perform a more careful data selection and avoid some of the problems experienced by this first pioneering effort to create a 3 dimensional model.

Hence, on the basis of the three models in Figure 19 and Table 4 we conclude that the upper limits on deviations from axial symmetry of the forward shock surface under average solar wind conditions are $\sim 1°$ in orientation and $\sim 1\,R_e$ in offset along the y' axis. This is not to say that when the interplanetary magnetic field is relatively strong (e.g., $\beta \lesssim 1$, $M_A \lesssim 5$, and $Q \lesssim 25$) the bow wave will remain axisymmetric in the face of large nonaxially symmetric magnetic stresses. However, it does state that the typical strength of the IMF is insufficient to cause large deviations from axial symmetry. In addition, it should be noted again that the presence of the spiral magnetic field in the solar wind should result in a nonaxially symmetric Mach cone [e.g., *Dryer and Heckman*, 1967] as has been observed by *Whang and Ness* [1970] at the Moon and possibly *Romanov et al.* [1978] at Venus. Thus further downstream than considered here, where shock position is becoming limited by the fast wave signal speed which is a function of $\vec{B}$, it may still be expected that the effect of the IMF on bow wave shape will be apparent.

The location of the bow shocks of the terrestrial planets have been scaled to a single dynamic pressure at 1 AU of 3.5×10^{-8} dynes/cm^2 in Figure 20 which corresponds to 1.5×10^{-8} at 1.5 AU, the mean dynamic pressure during the Mars observations used to create the shock model in Figure 16 [*Dolginov et al.*, 1976; *Dolginov*, 1978*a*]. In this way we have avoided scaling the size of the Martian obstacle with pressure because of its unknown response to upstream conditions. The mean, or possibly solar cycle average, bow wave for Venus is plotted with its weak dependence upon dynamic pressure [*Slavin et al.*, 1980] assumed negligible relative to the scale of the figure. At Mercury the uneroded solar wind stand-off distance of *Slavin and Holzer* [1979] has been scaled to a pressure of 14×10^{-8} dynes/cm^2 assuming a sixth root pressure dependence. The width of the magnetosheath and eccentricity have been increased slightly relative to the terrestrial case due to the lower Mach number conditions listed in Table 2 for 0.3–0.5 AU in order to give a qualitatively correct picture of the Hermaean bow wave. Finally, the mean earth bow shock from this study is also shown after being scaled to the indicated common pressure. Displayed in this way the immense size of the terrestrial magnetosphere relative to the obstacles to the solar wind at the other terrestrial planets is quite evident. In addition, when combined with the existence of compressional [*Siscoe et al.*, 1969] and shocklike features [*Schubert and Lichtenstein*, 1974] in

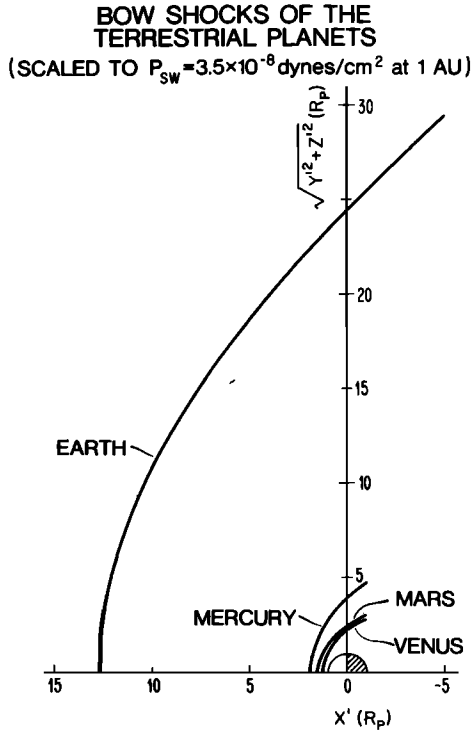

Fig. 20. The bow shocks of all four terrestrial planets are plotted in terms of planetary radii to show their relative stand-off distances. In the case of Venus the mean shock position from Venera and PVO, which may represent a solar cycle average, is displayed. For Mercury the bow wave surface shown is based upon the uneroded obstacle height determined by *Slavin and Holzer* [1979] with the magnetosheath thickness and eccentricity increased slightly relative to the terrestrial case to give a qualitative representation of the expected reduced Mach number conditions at 0.3–0.5 AU.

the solar wind flow about the limbs of the Moon and the vast bow waves of Jupiter and Saturn, this figure points up the large range in scale lengths over which the solar wind exhibits fluid characteristics. Mercury, while possessing an effective obstacle of greater diameter than Mars and Venus, is still much closer in size to those planets than to earth. It is also noted that the average location of the Cytherean bow wave is at a lower relative altitude than that of Mars but that near solar maximum their positions become comparable as judged by the Pioneer Venus results. This finding weakens the argument that Mars possesses a significant intrinsic magnetic moment simply due to its bow wave stand-off distance being greater than that observed at Venus near solar minimum by Venera 9 and 10 [see *Slavin and Holzer*, 1981]. Finally, it remains to be determined by both theoretical and observational studies to what degree the different absolute shock dimensions displayed in Figure 20 affect the physical processes of the foreshock, main transition layer, and magnetosheath.

Figure 21 complements the preceding view, which examined the relative sizes of the bow waves, by scaling the subsolar point on each to unity for the purpose of comparing their respective shapes. Each of the planets is displayed to provide a measure of the scaling factor. This would be equivalent to plotting the shock waves in units of obstacle radii if it were not for the fact that magnetosheath thickness varies with obstacle shape. As shown, the terrestrial bow wave flares out from the symmetry axis more than those of Venus and finally Mars. This is in contrast to the ϵ–L models used in a preliminary study by *Slavin et al.* [1979*a*] with a more restricted data set which could not detect the difference in shape between the Venus and earth bow stocks. Thus, using the same three parameter model in each case it is found that Mars possesses the most slender bow wave followed by Venus and earth in that order. The rms

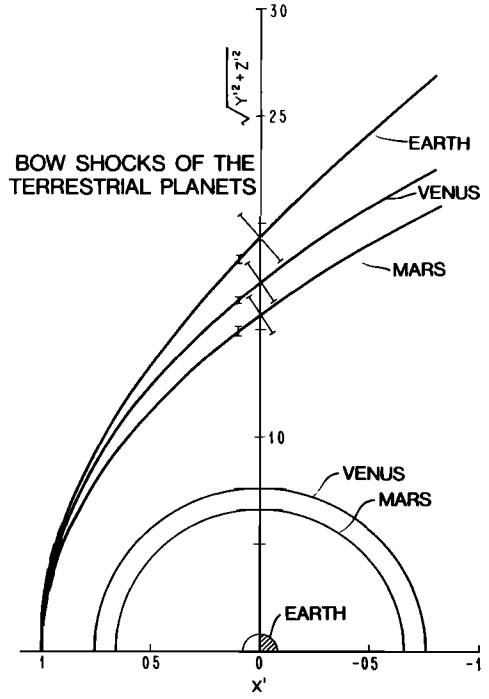

Fig. 21. The bow shocks of Venus, earth, and Mars have been scaled so their subsolar points are all the same distance from the center of their respective planets for ease in comparing the relative shapes of these three bow waves. The error bars normal to the shock surfaces give the rms deviations of the observations from the model boundaries while the smaller bars parallel to the vertical axis represent the uncertainty in the best fit.

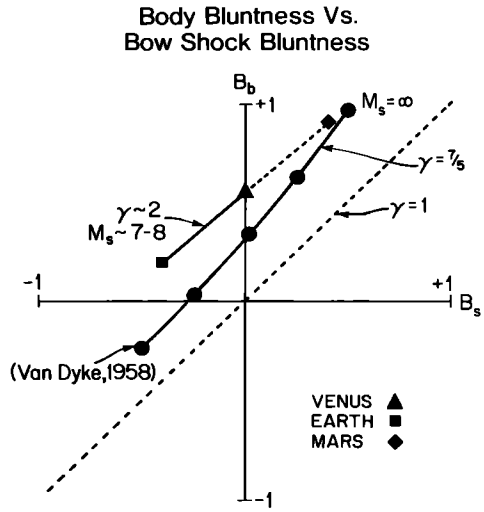

Fig. 22. The effective bluntnesses (i.e., $1-\epsilon^2$) of the obstacle surfaces at Venus and earth are plotted against bow shock bluntness with a linear extrapolation to Martian system indicated. Also displayed are the gasdynamic results of *Van Dyke* [1958] for $\gamma = 7/5, M_s = \infty$ as well as the limiting case of $\gamma = 1, M_s = \infty$. In this way, the observations of flow past the terrestrial planets appear qualitatively well ordered by existing blunt body hypersonic aerodynamic theory.

deviations displayed are similar, with the high compressibility of the terrestrial obstacle producing only a marginally greater variability in shock position than found at Venus and Mars.

As will be considered in detail in part 2 of this study, these findings have implications for the nature of flow past these planets. In the final figure the relationship between the shock and obstacle shapes is examined in terms of a bluntness parameter introduced by *Van Dyke* [1958] for the purpose of parameterizing gasdynamic shock/obstacle shape

$$B = 1 - \epsilon^2 \tag{9}$$

In terms of this parameter a spherical surface corresponds to $B = 1$, while ellipsoids have $B > 0$ and hyperboloids $B < 0$. In the limit of infinite Mach number the density jump across a normal gasdynamic shock goes as $(\gamma + 1)/(\gamma - 1)$, where γ is the usual ratio of specific heats at constant pressure and volume. *Spreiter et al.* [1966] found that the subsolar thickness of the magnetosheath was proportional to $(\gamma - 1)/(\gamma + 1)$ consistent with the need to conserve mass in the magnetosheath flow. Thus in the limit of infinite Mach number and infinite thermodynamic degrees of freedom (i.e., $\gamma = (n + 2)/n$, where n = number of degrees of freedom) the jump in density becomes infinite with the shock degenerating into an infinitesimal layer adjacent to the obstacle so that the shock and obstacle have identical shapes (i.e., $B_b = B_s$) as shown by the dashed line with a slope of unity in Figure 22. Also displayed is the gasdynamic relationship between shock bluntness B_s and the obstacle or body bluntness B_b for $M_s = \infty$ and $\gamma = 7/5$ from Van Dyke's study. Insofar as gasdynamics has applicability to the mean flow about the planets, it is possible to include Venus, earth, and Mars in this picture. Because the model determined eccentricity of a surface is dependent upon the point at which the focus is placed, it is necessary to create an effective eccentricity for each of the terrestrial planets referenced to a standard focus position. This has been done in Table 9 where the effective value of x_0 is taken somewhat arbitrarily to be 1/4 the shock stand-off distance which is near the mean for these planets. The body shapes at Venus and earth have been taken from the inopause/mantle-boundary layer [*Brace et al.*, 1980; *Spenner et*

TABE 9. Effective Bow Shock and Obstacle Shapes

Planet	$¼R_{ss}$	Effective Bow Shock	Eccentricity Obstacle	B_s	B_b
Venus	$0.33R_V$	1.0	0.65	0.0	+0.55
Earth	$3.5R_e$	1.2	0.9	−0.4	+0.2
Mars	$0.38R_{MS}$	0.8	0.3	+0.4	(+0.9)

The bluntness parameter of *Van Dyke* [1958], $B = 1 - \epsilon^2$, has been used to characterize the shapes of the bow waves at Venus, earth, and Mars as well as the Cytherean mantle/ionopause, the terrestrial magnetopause, and, by linear extrapolation, the obstacle to the solar wind at Mars (see Figure 21).

al., 1980; *Perez-de-Tejada*, 1980] and magnetopause [e.g., *Fairfield*, 1971; *Holzer and Slavin*, 1978; *Formisano et al.*, 1979] model surfaces. In the case of Mars we lack the in situ observations to determine the obstacle shape directly (e.g., *Slavin and Holzer* [1981] and references therein). However, a qualitative determination of shape is implied by the linear extrapolation from the Venus and earth results shown with a dashed line. Inspection of Figure 22 shows that our modeling results appear consistent with the gasdynamic expectations for a hypersonic (i.e., $M_s \gtrsim 5$) flow with $\gamma > 7/5$ (e.g., $\gamma = 2$ if the interplanetary magnetic field removes one degree of freedom to leave only two) about three moderately blunt bodies. The three cases shown (i.e., Venus-earth-Mars in the solar wind, an ideal gas with $\gamma = 7/5$ and $M_s = \infty$, and an ideal gas with $\gamma = 1$ and $M_s = \infty$) differ mostly in the adiabatic exponent γ appropriate to each of the fluids. As the γ factor increases from the degenerate $\gamma = 1$ situation, the sheath region between the shock and the obstacle increases in width everywhere and increases the rate at which it widens with growing distance downstream. The net effect in Figure 22 is that for a given eccentricity obstacle surface, the eccentricity of the resultant bow wave increases with increasing γ. Hence the $\gamma \sim 2$ trace appropriate to planets in the solar wind is displaced upward on the $\gamma = 7/5$ case for a gas with five degrees of freedom. In Part 2 of this study the ability of existing flow models to match these observations quantitatively and the implications for the solar wind interaction with the terrestrial planets is examined in detail.

CONCLUSIONS

1. The three parameter second order shock model method used in this study produces good fits to the forward portions of the bow wave surfaces at Venus, earth, and Mars. Discrepancies among the various second order fits that have been proposed appear to be due more to differences in the regions included in the models than in the modeling techniques and assumptions employed (e.g., inclusion of distant downstream shock crossings will force the model surface to have $\epsilon > 1$ independent of the actual shape of the near planet bow wave).

2. After scaling for the effects of differing solar wind dynamic pressure, the terrestrial bow wave showed only minor variations in position and shape during the period 1965–1972. This finding supports the similar conclusion reached by *Egidi et al.* [1970] reached by comparing the position of the bow shock seen near solar minimum by Imp 1 with the solar maximum observations of Heos 1. It is further found by this study that the variations in shock stand-off distance and shape remaining after correcting for P_{sw} are ordered by the sonic Mach number and not M_A, $M_{MS\|}$, or $M_{MS\perp}$ in agreement with the gasdynamic approximations of *Spreiter et al.* [1966] and *Dryer and Heckman* [1967]. In contrast, the Venus bow shock became significantly more distant between 1975 and 1979. This change has been attributed by *Slavin et al.* [1979*b*, 1980] to a solar cycle related variation in the solar wind interaction with that planet.

3. Examination of the earth shock crossings showed no significant east-west asymmetry in the bow wave orientation and y' coordinate offset of the focus at the $\sim 1°$ and $\sim 1 R_e$ levels in approximate agreement with the previous studies by *Gosling et al.* [1967], *Fairfield* [1971], and the unnormalized model of *Formisano* [1979]. Further, given the large variability of the IMF orientation about the Parker spiral angle and the typical values of $\beta = 1 - 2$ and $M_A = 8-10$ at 1 AU in contrast the smaller values assumed by *Walters* [1964], it is not clear that any theoretical grounds exist for expecting an east-west asymmetry in the average earth's bow shock larger than the limits set down above. It remains to be shown that they exist during low M_A and β conditions when the IMF is strong. This problem is currently under study with a significantly larger observational data base.

4. Mapping of the Pioneer Venus and Imp 4 bow shock crossings into the aberrated terminator plane relative to the transverse component of the IMF produced no significant deviations from axial symmetry contrary to the predictions of *Cloutier* [1976] and the experimental findings of *Verigin et al.* [1977] using a small Venera data set. It is suggested that the Venera results are associated with asymmetric Mach cone effects due to the use of distant downstream crossings in that study.

5. Finally, in shape the forward portion (i.e., $x > -1 R_{ob}$) of the Mars shock is the least blunt followed by the shocks of Venus and the earth, respectively, implying the same order for the bluntnesses of their respective obstacles. Part 2 of this study will examine the ability of existing gasdynamic and MHD flow calculations to model these results and consider the implications for their respective interactions with the solar wind.

Acknowledgments. The authors wish to thank D. H. Fairfield and the NSSDC for a listing of Imp 3 and 4 bow wave crossings, O. L. Vaisberg and V. N. Smirnov for the Prognoz 1 and 2, Venera 9 and 10, and Mars 2, 3, and 5 shock data, and V. Formisano for the Heos 1 shock encounter data set. In addition, we have made use of the UCLA Pioneer Venus magnetometer observations, C. T. Russell, principal investigator. This research has been supported by NASA grant NAGW-74.

REFERENCES

Auer, R.-D., MHD aspects of the earth's bow shock, 2, Motions induced by directional discontinuities, *J. Geophys. Res.*, *79*, 5121, 1974.

Bavassano, B., F. Mariani, U. Villante, and N. F. Ness, Multiple crossings of the earth's bow shock at large geocentric distances, *J. Geophys. Res.*, *76*, 5970, 1971.

Bogdanov, A. V., and O. L. Vaisberg, Structure and variations of the solar wind-Mars interaction region, *J. Geophys. Res.*, *80*, 487, 1975.

Bonifazi, C., A. Egidi, G. Moreno, and S. Orsini, Backstreaming ions outside the earth's bow shock and their interactions with the solar wind, *J. Geophys. Res.*, *85*, 3461, 1980.

Brace, L. H., R. F. Theis, W. R. Hoegy, J. H. Wolfe, J. D. Mihalov, C. T. Russell, R. C. Elphic, and A. F. Nagy, The dynamic behavior of the Venus ionosphere in response to solar wind interactions, *J. Geophys. Res.*, *85*, 7663, 1980.

Breus, T. K., Venus: Review of present understanding of solar wind interaction, *Space Sci. Rev.*, *23*, 153, 1979.

Chao, J. K., and M. J. Wiskerchen, The ratio of specific heats for post-shock plasmas of a detached bow shock: An MHD model, *J. Geophys. Res., 79,* 4769, 1974.

Cloutier, P. A., Solar wind interaction with planetary ionospheres, in *Solar Wind Interactions with the Planets Mercury, Venus, and Mars,* edited by N. F. Ness, *NASA SP-397,* pp. 111–119, 1976.

Diodatio, L., G. Moreno, G. Signorini, and K. W. Ogilvie, Long-term variations of the solar wind plasma parameters, *J. Geophys. Res., 79,* 5095, 1974.

Dolginov, Sh. Sh., On the magnetic field of Mars: Mars 2 and 3 evidence, *Geophys. Res. Lett., 5,* 89, 1978*a*.

Dolginov, Sh. Sh., On the magnetic field of Mars: Mars 5 evidence, *Geophys. Res. Lett., 5,* 93, 1978*b*.

Dolginov, Sh. Sh., E. G. Eroshenko, D. N. Zhuzgov, V. A. Sharova, K. I. Gringauz, V. V. Bezrukikh, T. K. Breus, M. I. Verigin, and A. P. Remizov, Magnetic field and plasma inside and outside of the Martian magnetosphee, in *Solar Wind Interaction with the Planets Mercury, Venus, and Mars,* edited by N. F. Ness, *NASA SP-397,* pp. 1–20, 1976.

Dryer, M., Solar wind interactions-hypersonic analogue, *Cosmic Electrodyn., 1,* 115, 1970.

Dryer, M., and R. Faye-Petersen, Magnetogasdynamic boundary condition for a self-consistent solution to the closed magnetopause, *AIAA J., 4,* 246, 1966.

Dryer, M., and G. R. Heckman, Application of the hypersonic analogue to the standing shock of Mars, *Solar Phys., 2,* 112, 1967.

Egidi, A., V. Formisano, F. Palmiotto, P. Saraceno, and G. Moreno, Solar wind and location of shock front and magnetopause at the 1969 solar maximum, *J. Geophys. Res., 75,* 6999, 1970.

Fairfield, D. H., Average and unusual locations of the earth's magnetopause and bow shock, *J. Geophys. Res., 76,* 6700, 1971.

Fairfield, D. H., Global aspects of the earth's magnetopause, Proceedings of the Magnetospheric Boundary Layers Conference, *ESA SP-148,* Evr. space agency, 1979.

Fairfield, D. H., and K. W. Behannon, Bow shock and magnetosheath waves at Mercury, *J. Geophys. Res., 81,* 3897, 1976.

Formisano, V., Orientation and shape of the earth's bow shock in three dimensions, *Planet. Space Sci., 27,* 1151, 1979.

Formisano, V., P. C. Hedgecock, G. Moreno, F. Palmiotto, and J. K. Chao, Solar wind interaction with the earth's magnetic field, 2, MHD bow shock, *J. Geophys. Res., 78,* 3731, 1973.

Gazis, P. R., A. J. Lazarus, and J. D. Sullivan, Voyager observations of solar wind temperature 1–10 AU (abstract), *Eos Trans. 62,* 378, 1981.

Gosling, J. T., and S. J. Bame, Solar wind speed variations: An autocorrelation analysis, *J. Geophys. Res., 77,* 12, 1972.

Gosling, J., J. R. Asbridge, S. J. Bame, and I. Strong, Vela 2 measurements of the magnetopause and bow shock positions, *J. Geophys. Res., 72,* 101, 1967.

Greenstadt, E. W., Dependence of shock structure at Venus and Mars on orientation of the IMF, *Cosmic Electrodyn., 1,* 380, 1970.

Greenstadt, E. W., P. C. Hedgecock, and C. T. Russell, Large-scale coherence and high velocities of the earth's bow shock on February 12, 1969, *J. Geophys. Res., 77,* 1116, 1972.

Gringauz, K. I., Report on 18th COSPAR meeting, *Rep. D-194,* Space Res. Inst., Moscow, 1975.

Gringauz, K. I., V. V. Bezrukikh, M. I. Verigin, and A. P. Remizov, Studies of the solar plasma near Mars and on the earth-Mars route using charged particle traps on Soviet spacecraft in 1971–3, *Cosmic Res., 13,* 107, 1975.

Gringauz, K. I., V. V. Bezrukikh, M. I. Verigin, and A. P. Remizov, On the electron and ion components of plasma in the antisolar part of near-Martian space, *J. Geophys. Res., 81,* 3349, 1976.

Gringauz, K. I., A comparison of the magnetospheres of Mars, Venus, and the Earth, *Physics of Planetary Magnetospheres,* vol. 1, Proceedings of Symposium 3 of the 23rd Plenary Meeting of COSPAR, edited by K. Knott, pp. 5-24, Budapest, 1980.

Holzer, R. E., and J. A. Slavin, Magnetic flux transfer associated with expansions and contractions of the dayside magnetosphere, *J. Geophys. Res., 83,* 3831, 1978.

Holzer, R. E., and J. A. Slavin, The effect of solar wind structure on magnetospheric energy supply during solar cycle 20, *J. Geophys. Res., 86,* 675, 1981.

Holzer, R. E., M. G. McLeod, and E. J. Smith, Preliminary results from the Ogo 1 search coil magnetometer:Boundary positions and magnetic noise spectra, *J. Geophys. Res., 71,* 1481, 1966.

Holzer, R. E., T. G. Northrop, J. V. Olson, and C. T. Russell, Study of waves in the earth's bow shock, *J. Geophys. Res., 77,* 2264, 1972.

Howe, H. C., Jr., and J. H. Binsack, Explorer 33 and 35 plasma observations of magnetosheath flow, *J. Geophys. Res., 77,* 334, 1972.

Hundhausen, A. J., S. J. Bame, and J. R. Asbridge, Plasma flow pattern in the magnetosheath, *J. Geophys. Res., 74,* 2799, 1969.

King, J. H., *Interplanetary Medium Data Book, Rep. NSSDC 7704,* NASA Goddard Space Flight Center, Greenbelt, Md., 1977.

King, J. H., Solar cycle variations in IMF intensity, *J. Geophys. Res., 84,* 5938, 1979.

Michel, F. C., Detectability of disturbances in the solar wind, *J. Geophys. Res., 70,* 1, 1965.

Ness, N. F., The magnetic fields of Mercury, Mars, and the Moon, *Ann. Rev. Earth Planet, Sci., 7,* 249, 1979.

Ness, N. F., K. W. Behannon, R. P. Lepping, and Y. C. Whang, The magnetic field of Mercury, *J. Geophys. Res., 80,* 2708, 1975.

Olilvie, K. W., J. D. Scudder, V. M. Vasyliunas, R. E. Hartle, and G. L. Siscoe, Observations at the planet Mercury by the plasma electron experiment, *J. Geophys. Res., 82,* 1807, 1977.

Olson, J. V., and R. E. Holzer, On the local time dependence of the bow shock wave structure, *J. Geophys. Res., 79,* 939, 1974.

Perez-de-Tejada, H., Evidence for a viscous boundary layer at the Venus inopause from the preliminary Pioneer Venus results, *J. Geophys. Res., 85,* 7709, 1980.

Romanov, S. A., V. N. Smirnov, and O. L. Vaisberg, Interaction of the solar wind with Venus, *Cosmic Res., 16,* 603, 1978.

Russell, C. T., On the relative locations of the bow shocks of the terrestrial planets, *Geophys. Res. Lett., 4,* 387, 1977.

Russell, C. T., The magnetic field of Mars: Mars 3 evidence reexamined, *Geophys. Res. Lett., 5,* 81, 1978*a*.

Russell, C. T., The magnetic field of Mars: Mars 5 evidence reexamined, *Geophys. Res. Lett., 5,* 85, 1978*b*.

Russell, C. t., The interaction of the solar wind with Mars, Venus, and Mercury, in *Solar System Plasma Physics,* vol. 2, edited by C. F. Kennel, L. J. Lanzerotti, and E. N. Parker, pp. 208–252, North-Holland, Amsterdam, 1979.

Russell, C. T., and E. W. Greenstadt, Initial Isee magnetometer results: Shock observations, *Space Sci. Rev., 23,* 3, 1979.

Schubert, G., and B. R. Lichtenstein, Observations of moon-plasma interactions by orbital and surface experiments, *Rev. Geophys. Space Phys., 12,* 592, 1974.

Shen, W.-W., The earth's bow shock in an oblique interplanetary field, *Cosmic Electrodyn., 2,* 381, 1972.

Siscoe, G. L., E. F. Lyon, J. H. Binsack, and H. S. Bridge, Experimental evidence for a detached lunar compression wave, *J. Geophys. Res., 74,* 59, 1969.

Siscoe, G. L., and J. A. Slavin, Planetary magnetospheres, *Rev. Geophys. Space Phys., 17,* 1677, 1979.

Sittler, E. C., Jr., and J. D. Scudder, An empirical polytrope law for solar wind thermal electrons between 0.45 and 4.76 AU: Voyager 2 and Mariner 10, *J. Geophys. Res., 85,* 5131, 1980.

Slavin, J. A., and R. E. Holzer, The effect of erosion on the solar wind stand-off distance at Mercury, *J. Geophys. Res., 84,* 2076, 1979.

Slavin, J. A., and R. E. Holzer, The solar wind interaction with Mars revisted, *J. Geophys. Res., in press, 1981.*

Slavin, J. A., R. C. Elphic, C. T. Russell, J. H. Wolfe, and D. S. Intriligator, Position and shape of the Venus bow shock: Pioneer Venus orbiter observations, *Geophys. Res. Lett., 6,* 901, 1979*a*.

Slavin, J. A., R. C. Elphic, and C. T. Russell, A comparison of Pioneer Venus and Venera bow shock observations: Evidence for a solar cycle variation, *Geophys. Res. Lett., 6,* 905, 1979*b*.

Slavin, J. A., R. C. Elphic, C. T. Russell, F. L. Scarf, J. H. Wolfe, J. D. Mihalov, D. S. Intriligator, L. H. Brace, H. A. Taylor, Jr., and R. E. Daniell, Jr., The solar wind interaction with Venus: Pioneer Venus observation of bow shock location and structure, *J. Geophys. Res., 85,* 7625, 1980.

Smith, E. J., Planetary magnetic field experiments, in *Advanced Space Environments,* edited by O. L. Tiffany and E. M. Zaitzeff, American Astronautical Society, Tarzana, Calif., 1969.

Smirnov, V. N., O. L. Vaisberg, and D. S. Intriligator, An empirical model of the Venusian outer environment, 2, The shape and location of the bow shock, *J. Geophys. Res., 85,* 7651, 1980.

Spenner, K., W. C. Knudsen, K. L. Miller, V. Novak, C. T. Russell, and R. C. Elphic, Observation of the Venus mantle, The boundary region between the solar wind and ionosphere, *J. Geophys. Res., 85,* 7655m 1980.

Spreiter, J. R., and A. Y. Alksne, Solar wind flow past objects in the solar system, *Ann. Rev. Fluid Mech., 8,* 313, 1970.

Spreiter, J. R., and W. P. Jones, On the effect of a weak interplanetary

magnetic field on the interaction between the solar wind and geomagnetic field, *J. Geophys. Res., 68,* 3555, 1963.

Spreiter, J. R., and A. W. Rizzi, Aligned MHD solution for solar wind flow past the earth's magnetosphere, *Acta Astronaut., 1,* 15, 1974.

Spreiter, J. R., and S. S. Stahara, A new predictive model for determining solar wind-terrestrial planet interactions, *J. Geophys. Res., 85,* 6769, 1980*a*.

Spreiter, J. R., and S. S. Stahara, Solar wind flow past Venus: Theory and comparison, *J. Geophys. Res., 85,* 7715, 1980*b*.

Spreiter, J. R., A. L. Summers, and A. Y. Alksne, hydromagnetic flow around the magnetosphere, *Planet. Space Sci., 14,* 223, 1966.

Theis, R. F., L. H. Brace, and H. G. Mayr, Empirical models of electron temperature and density in the Venus ionosphere, *J. Geophys. Res., 85,* 7787, 1980*a*.

Theis, R. F., L. H. Brace, K. H. Schatten, C. T. Russell, J. A. Slavin, and J. H. Wolfe, The Venus ionosphere as an obstacle to the solar wind, *Physics of Planetary Magnetospheres,* vol. 1, Proceedings of Symposium 3 of the 23rd Plenary Meeting of COSPAR, edited by K. Knott, pp. 47–60, Budapest, 1980.

Vaisberg, O. L., Mars-plasma environment, in *Physics of Solar Planetary Environments,* edited by D. J. Williams, pp. 854–871, Wasington, D. C., 1976.

Vaisberg, O. L., A. V. Bogdanov, V. N. Smirnov, and S. A. Romanov, On the nature of the solar wind Mars interaction, in *Solar Wind Interaction With the Planets Mercury, Venus, and Mars,* edited by N. F. Ness, pp. 21–40, *NASA SP-397,* 1976.

Van Dyke, M. D., The supersonic blunt body problem—Review and extension, *J. AeroSp. Sci., 29,* 485, 1958.

Verigin, M. I., K. I. Gringauz, T. Gombosi, T. K. Breus, V. V. Bezrukikh, A. P. Remizov, and G. I. Volkov, Plasma near Venus from the Venera 9 and 10 wide-angle plasma analyzer data, *J. Geophys. Res., 83,* 3721, 1978.

Walters, G. K., Effect of oblique interplanetary magnetic field on the shape and behavior of the magnetosphere, *J. Geophys. Res., 69,* 1769, 1964.

Whang, Y. C., and N. F. Ness, Observations and interpretations of the lunar Mach cone, *J. Geophys. Res., 75,* 6002, 1970.

Wolfe, J. H., The large scale structure of the solar wind, in *Solar Wind,* edited by C. P. Sonett, P. J. Coleman, Jr., and J. M. Wilcox, pp. 170, *NASA SP-308,* 1972.

Wolff, R. S., B. E. Goldstein, and S. Kumar, A model of the variability of the Venus ionopause altitude, Geophys. Res. Lett., *6,* 7641, 1979.

Zhuang, H. C., C. T. Russell, and R. J. Walker, The influence of the IMF and thermal pressure on the position and shape of the magnetopause, In press, *J. Geophys. Res.*, 1981.

(Received March 3, 1981;
revised July 8, 1981;
accepted July 9, 1981.)